

Predicting failure pressure of corroded gas pipelines: A data-driven approach using machine learning

Rui Xiao^{a,*}, Tarek Zayed^a, Mohamed A. Meguid^b, Laxmi Sushama^c

^a Department of Building and Real Estate, The Hong Kong Polytechnic University, Hung Hom, Kowloon, Hong Kong

^b Department of Civil Engineering, McGill University, Montreal, QC H3A 0C3, Canada

^c Department of Civil Engineering, Trottier Institute for Sustainability in Engineering and Design, McGill University, Montreal, QC, Canada

ARTICLE INFO

Keywords:

Pipeline integrity
Corroded pipelines
Failure pressure
Machine learning
Shapley additive explanations

ABSTRACT

This paper presents a novel methodology utilizing machine learning (ML) techniques to accurately forecast the failure pressure of corroded pipelines, which are pivotal for oil, gas, and petroleum product transport. In contrast to prior approaches, this study overcomes their limitations by integrating physically significant factors tied to corroded pipeline failure mechanisms and delivering interpretable models. Robust ML models are constructed using dependable experimental data from pertinent literature sources, ensuring research rigor. To bolster model interpretability, the SHAP method is deployed, facilitating a comprehensive grasp of each feature's impact on predictions. The performance and efficacy of the developed ML models are rigorously assessed using real-world pipeline incidents reported by the PHMSA in the US, further validating their practical utility. The findings not only affirm the models' precision and dependability but also yield valuable insights, underscoring their importance. This study makes a substantial contribution to the enhancement of pipeline integrity management by enabling precise failure pressure predictions in corroded pipelines. The insights gleaned from this research hold practical implications, enabling well-informed choices in pipeline design, integrity management, and risk assessment. Thus, it stands as a valuable resource for pipeline operators aiming to optimize resource allocation and bolster overall pipeline safety and efficiency.

1. Introduction

Pipelines are crucial for the transportation of oil, gas, and petroleum products due to their economic efficiency, safety, and reliability advantages over other modes of transportation (Amaya-Gómez et al., 2019a; Manservigi et al., 2022; Muhlbauer, 2006). However, pipeline failures can lead to substantial resource losses, economic damages, and safety risks. In the United States alone, gas pipeline incidents have resulted in injuries, fatalities, and substantial costs. Corrosion is a major contributor to these incidents (Halim et al., 2020). To combat corrosion, technologies like cathodic protection systems and pipe cleaning methods have been deployed for both new and existing pipelines (Ma et al., 2023b). As a result, the establishment and implementation of pipeline integrity management have become pivotal for safe and efficient pipeline operation (Amaya-Gómez et al., 2019b). Risk assessment, involving risk analysis and control, plays a vital role in evaluating pipeline integrity, particularly in estimating the reliability of pipelines susceptible to corrosion. This estimation helps predict remaining service

life and failure probabilities, facilitating optimized resource allocation for inspection, repair, and maintenance activities (Khan et al., 2021; Ma et al., 2022). Typically, a limit state function is employed to assess reliability, with residual strength subjected to corrosion being a key load parameter (Wang et al., 2019, 2023). Therefore, accurately predicting the failure pressure of corroded pipelines is essential for precise reliability assessment and efficient resource allocation in the management of pipeline integrity.

To date, numerous studies have aimed to predict the failure pressure of corroded pipelines, employing either experimental or numerical approaches. These endeavors have led to the development of various codes and standards, which rely on experimental tests or finite element simulations to guide the estimation of failure pressure. Notable methods include: 1) NG-18 equations based on fracture mechanics theory by the American Gas Association (Kiefner et al., 1973), encompassing ASME B31G (Li et al., 2023; Manual for determining the remaining strength of corroded pipelines, 2012) modified ASME B31G (Manual for determining the remaining strength of corroded pipelines, 2012), SHELL 92

* Corresponding author.

E-mail address: ruixiao@polyu.edu.hk (R. Xiao).

(Ritchie and Last, 1995), Rectangular Parabolic Area (RPA) (Benjamin and Andrade, 2003), DNV RP-F101 (LPC) (“[DNV-RP-F101 Corroded pipelines](#),” 2015), Canadian Standards Association (CSA) Z662 (CSA, Z662:19, Oil and gas pipeline systems, 2019), FITNET FSS (Koçak et al., 2008); 2) approaches based on Buckingham’s π theorem, such as Netto’s model (Netto et al., 2005); 3) models utilizing the Pipe Corrosion Criterion approach, including PCORRC (Stephens and Leis, 2000) and modified PCORRC (Yeom et al., 2015a); and 4) models developed using other methods such as RAM PIPE REQUAL (Bea, 1999). Choi et al. derived a limit load solution for evaluating corrosion in X65 gas pipelines, based on a series of burst tests and finite element simulations (Choi et al., 2003). Additionally, Shuai et al. proposed the “CUP” model for predicting failure pressure in corroded pipelines using the finite element method (FEM) (Shuai et al., 2017). These empirical formulas have gained wide adoption in engineering practice due to their computational convenience. However, it is important to note that these models are often formulated based on limited experimental tests or specific pipeline strength, making them less suitable for accurately predicting failure pressures in high-strength pipelines. Moreover, their prediction results tend to be conservative compared to actual failure pressures, leading to unnecessary resource waste in inspection, repair, and maintenance activities.

In recent years, the Finite Element Method (FEM) has gained prominence as a tool for accurately predicting the failure pressure of corroded pipelines, owing to advancements in computer technology and numerical simulation techniques. While previous research has predominantly focused on pipelines with low to moderate strength pipelines (Choi et al., 2003; Netto et al., 2005), a subset of studies has explored the failure behavior of high-strength pipelines. For instance, Yeom et al. conducted a comprehensive investigation into the failure characteristics of an API X70 pipeline containing single corrosion defects of varying dimensions using nonlinear FEM, validating their results against hydrostatic burst tests (Yeom et al., 2015b). This led to the development of a conservative evaluation equation tailored to single corrosion defects, ensuring the integrity of corroded pipelines. Similarly, Chen et al. used nonlinear FEM to assess high-strength pipeline failure pressures, providing regression equations and extending their analysis to pipelines with multiple corruptions, demonstrating superior accuracy compared to alternative methods (Chen et al., 2015). Bhardwaj et al. explored the less-studied influence of the strain hardening rate on corroded pipeline remaining strength, developing practical models validated through experimental tests (Bhardwaj et al., 2021). However, while FEM offers robust insights into corroded pipeline behavior, its practical utility for rapid pipeline integrity assessments is constrained by simplifications, assumptions, grid resolution, and the dynamic nature of corrosion in real-world scenarios.

The rapid proliferation of artificial intelligence (AI) and its extensive integration into various research domains has ushered in an era of data-driven methodologies (Dawood et al., 2020; Zio, 2022). Notably, ML models, renowned for their proficiency in capturing intricate and nonlinear relationships, have surfaced as potent instruments for advancing risk assessment within infrastructure systems (Wang et al., 2022). In the context of forecasting the failure pressure of corroded pipelines, several studies have harnessed ML techniques. For instance, Silva et al. ingeniously amalgamated finite element analysis with artificial neural networks (ANN) to construct an ANN model, rooted in a meticulously generated dataset derived from finite element modeling (Silva et al., 2007), which, when combined with empirical data from the literature, enabled accurate predictions of failure pressures (Lo et al., 2021; Zhang et al., 2023). Deep neural networks (DNN) have exhibited exceptional precision and computational efficiency in forecasting corroded pipeline failure pressures (Oh et al., 2020; Su et al., 2021). A plethora of ML models have been explored, encompassing Phan and Dhar’s thorough investigation that favored support vector regression (SVR) and noted material-specific model limitations. Abyani et al. assessed six models, including ANN, support vector machine (SVM),

genetic programming (GP), random forest (RF), gaussian process regression (GPR), and K-nearest neighbor (KNN) (Abyani et al., 2022), while Ma et al. embraced ensemble methods like RF, XGBoost, and LightGBM, all of which outperformed conventional empirical formulas (Ma et al., 2023a). Additionally, various studies introduced the relevance vector machine (RVM), often coupled with the multi-objective salp swarm algorithm (MOSSA) for parameter optimization (Lu et al., 2021a). Principal component analysis (PCA) streamlined dimensionality, and SVM were fine-tuned to predict residual strength (Lu et al., 2021b). Most notably, Phan and Duong’s deployment of the Adaptive Neuro Fuzzy Inference System (ANFIS) in conjunction with PCA led to an ANFIS-PCA model that surpassed alternatives with an impressive correlation coefficient of 0.992 (Phan and Duong, 2021).

While extensive research has delved into predicting failure pressure in corroded pipelines, several critical research gaps persist, demanding a resolution to enhance prediction model performance. Primarily, the scarcity of experimental data for diverse steel grades has prompted the widespread use of FEM to create simulated datasets. However, the reliability and accuracy of FEM results come into question, given the intricate failure behavior observed in varying environmental contexts. This raises concerns about the applicability of research findings in practical scenarios. Additionally, existing studies have predominantly concentrated on conventional pipeline and defect parameters, largely overlooking the factors that reflect the underlying physical insights, such as relative thickness, which significantly influence pipeline failure, and the strain hardening effect has been recognized as having a substantive effect on the failure mechanisms of corroded gas pipelines (Zhu, 2021, 2023), but has not yet been incorporated into machine learning-based models for predicting burst pressure, as evidenced by the existing literature. Moreover, most ML models designed for predicting failure pressure in corroded pipelines operate as opaque “black-box” models, lacking transparency in their input-output relationships, which limits their utility in guiding pipeline design, risk mitigation, and improving reliability. Lastly, there is a notable gap in evaluating the applicability of these ML models with real-world field data, which presents an opportunity to gain valuable insights and validate their effectiveness in practical pipeline incidents.

Motivated by the aforementioned gaps, this study presents a methodology utilizing ML techniques to predict the failure pressure of corroded pipelines. The analysis focuses exclusively on the impact of internal pressure on corroded pipelines, as the influence of the backfill soil overburden load is considered relatively insignificant. Initially, experimental test results are gathered from existing literature to establish the foundation for developing ML models. Subsequently, a comprehensive set of significant features informed by domain-specific knowledge that encapsulates the intrinsic physical phenomena, in addition to the fundamental pipeline and defect parameters, are proposed to construct the feature vector, facilitating a more robust and accurate modeling of the relevant processes. Seven distinct ML models, namely ANN, SVR, KNN, Decision Trees (DT), RF, Adaboost, and Gradient Boosted Decision Trees (GBDT) are trained and validated using the collected dataset to predict the failure pressure of corroded pipelines. To enhance interpretability, the SHapley Additive exPlanations (SHAP) method is employed to elucidate the impact of each feature on the model’s prediction for both the entire dataset and individual samples. Finally, the applicability of the developed models is assessed using pipeline incidents reported by the Pipeline and Hazardous Materials Safety Administration (PHMSA) in the United States, enabling the derivation of meaningful conclusions.

2. Existing failure pressure models

This section will provide a brief introduction to the prevailing empirical codes and standards commonly utilized for predicting the failure pressure of corroded pipelines. Consider a pipeline characterized by an external diameter (D), thickness (t), yield strength (σ_y), and

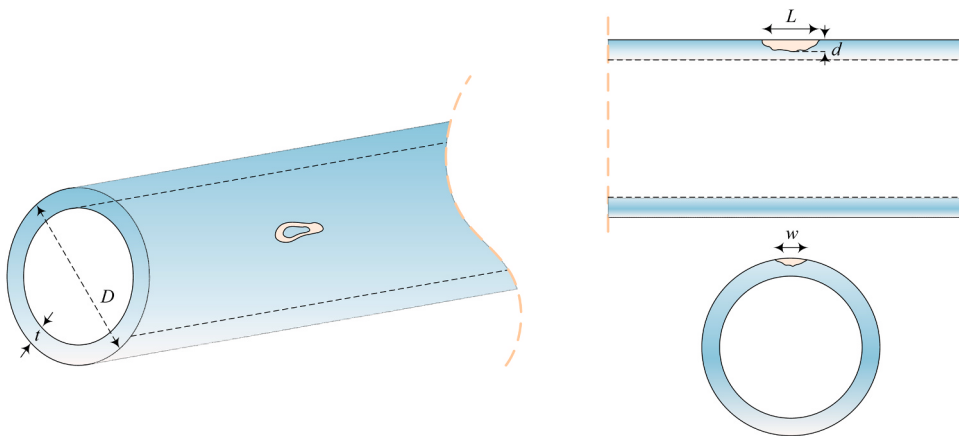


Fig. 1. Schematic diagram of a corroded pipeline.

Table 1
Folias bulging factors and limitations of existing models.

Category	Model	Folias Factor	Restriction
NG-18	ASME B31G	$M = \begin{cases} \frac{1 - \frac{2}{3}(d/t)}{1 - \frac{2}{3}(d/t) \cdot \sqrt{1 + 0.8\left(\frac{L}{\sqrt{Dt}}\right)^2}}, & \text{for } \frac{d}{t} \leq 0.8, \frac{L^2}{Dt} \leq 20 \\ 1 - \frac{d}{t}, & \text{for } \frac{d}{t} \leq 0.8, \frac{L^2}{Dt} > 20 \end{cases}$	<ul style="list-style-type: none"> For low strength pipelines (below X56) Parabolic shape defect
	Modified ASME B31G	$M = \begin{cases} \sqrt{1 + 0.6275\left(\frac{L}{\sqrt{Dt}}\right)^2} - 0.003375\left(\frac{L}{\sqrt{Dt}}\right)^4, & \text{for } \frac{d}{t} \leq 0.8, \frac{L^2}{Dt} \leq 50 \\ 3.3 + 0.032\left(\frac{L}{\sqrt{Dt}}\right)^2, & \text{for } \frac{d}{t} \leq 0.8, \frac{L^2}{Dt} > 50 \end{cases}$	<ul style="list-style-type: none"> For low and medium strength pipelines (below X65)
SHELL 92		$M = \sqrt{1 + 0.805\left(\frac{L}{\sqrt{Dt}}\right)^2}, \text{ for } \frac{d}{t} \leq 0.85$	<ul style="list-style-type: none"> Rectangular shape defect
RPA		$M = \begin{cases} \sqrt{1 + 0.6275\left(\frac{L}{\sqrt{Dt}}\right)^2} - 0.003375\left(\frac{L}{\sqrt{Dt}}\right)^4, & \text{for } \frac{L^2}{Dt} \leq 20 \\ 2.1 + 0.07\left(\frac{L}{\sqrt{Dt}}\right)^2, & \text{for } \frac{L^2}{Dt} > 20 \end{cases}$	<ul style="list-style-type: none"> For low and medium strength pipelines (below X65)
DNV RP-F101		$M = \sqrt{1 + 0.31\left(\frac{L}{\sqrt{Dt}}\right)^2}, \text{ for } \frac{d}{t} \leq 0.85$	<ul style="list-style-type: none"> For low and medium-strength pipelines Rectangular shape defect
CSA Z662		$M = \begin{cases} \sqrt{1 + 0.6275\left(\frac{L}{\sqrt{Dt}}\right)^2} - 0.003375\left(\frac{L}{\sqrt{Dt}}\right)^4, & \text{for } \frac{L^2}{Dt} \leq 50 \\ 3.3 + 0.032\left(\frac{L}{\sqrt{Dt}}\right)^2, & \text{for } \frac{L^2}{Dt} > 50 \end{cases}$	<ul style="list-style-type: none"> For low and medium strength pipelines (below X65)
FITNET FSS		$M = \sqrt{1 + 0.805\left(\frac{L}{\sqrt{Dt}}\right)^2}$	<ul style="list-style-type: none"> Rectangular shape defect
Buckingham's π theorem	Netto	/	<ul style="list-style-type: none"> For medium and high strength pipelines
Pipe Corrosion Criterion	PCORRC	/	<ul style="list-style-type: none"> Small database
	Modified PCORRC	/	<ul style="list-style-type: none"> For medium and high strength pipelines
Others	RAM PIPE REQUAL	/	<ul style="list-style-type: none"> For medium and high strength pipelines
	Choi	/	<ul style="list-style-type: none"> For low strength pipelines For X65 pipelines Rectangular shape defect
	CUP	/	<ul style="list-style-type: none"> For X46, X52 and X60 pipelines Small database

ultimate tensile strength (σ_u), and a corrosion defect with length (L), width (w) and depth (d) depicted in Fig. 1.

2.1. Models based on NG-18 equations

2.1.1. ASME B31G

ASME B31G is a conventional approach that relies on 47 full-scale burst pressure tests conducted on low-strength steel pipelines. This method assumes a parabolic shape for short defects and a rectangular

shape for long defects. The failure pressure can be estimated using the following equation (Manual for determining the remaining strength of corroded pipelines, 2012; Xie et al., 2023),

$$P_f = 2.2\sigma_y \frac{t}{D} M \quad (1)$$

where M represents the Folias bulging factor, and its corresponding expression can be found in Table 1.

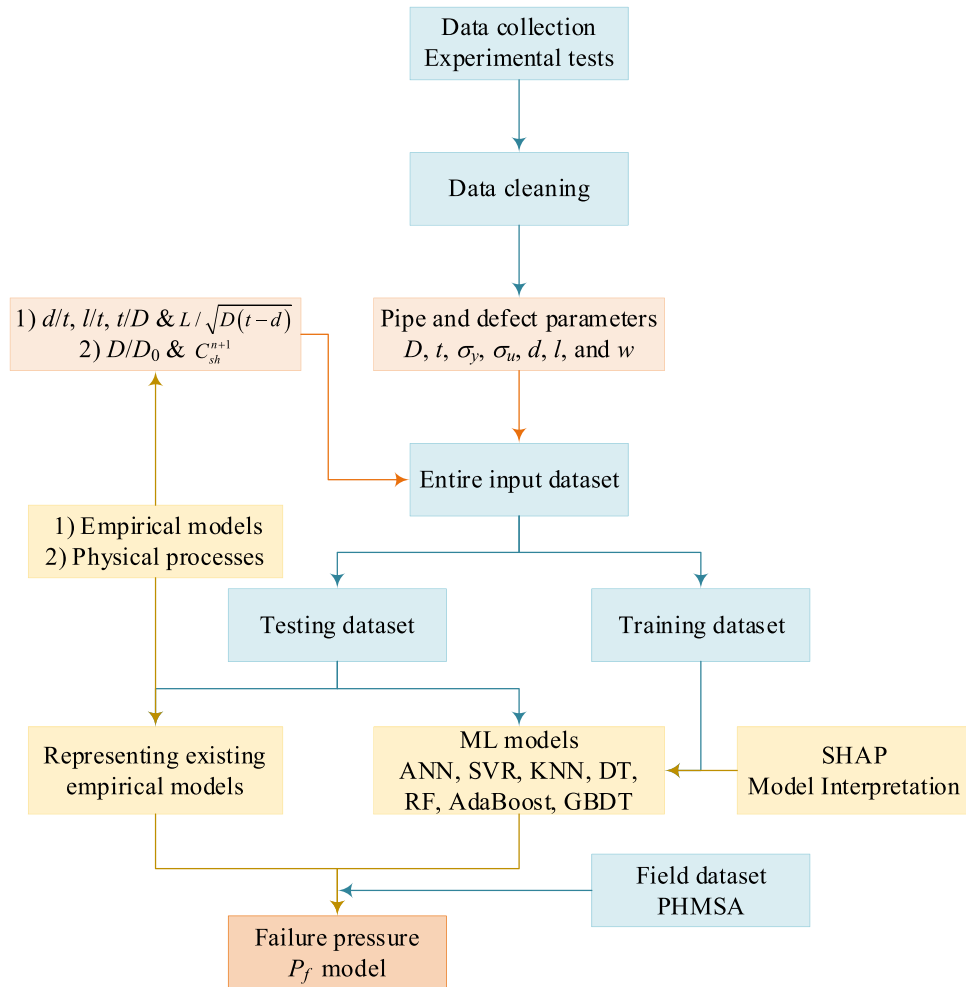


Fig. 2. The framework of the proposed method for predicting the failure pressure.

2.1.2. Modified ASME B31G (RSTRENG 0.85 dL)

The ASME B31G code has been found to be excessively conservative in real-world scenarios, leading to modifications made by Kiefner and Vieth through the RSTRENG code. These modifications were based on 86 full-scale burst pressure tests. The modified version of the code can be expressed as ([Manual for determining the remaining strength of corroded pipelines, 2012](#)),

$$P_f = 2(\sigma_y + 68.95) \frac{t}{D} \frac{1 - 0.85(d/t)}{1 - 0.85(d/t)/M} \quad (2)$$

2.1.3. SHELL 92

The SHELL92 model, developed by Ritchie and Last for Shell Oil Company, is a modification of the ASME B31G model. In this modified version, the defect is assumed to have a rectangular shape, and the consideration of ultimate tensile strength is introduced ([Ritchie and Last, 1995](#)),

$$P_f = 1.8 \frac{t}{D} \sigma_u \left(\frac{1 - (d/t)}{1 - (d/t)/M} \right) \quad (3)$$

2.1.4. RPA

The RPA model, developed by Benjamin and Andrade, is another modification of the Modified B31G model. It was specifically designed to address the unsatisfactory prediction results for long corrosion defects and developed based on the analysis of nine burst tests conducted on pipelines with long uniform depth corrosion defects. The expression for the RPA model is provided as ([Benjamin and Andrade, 2003](#)),

$$P_f = 2(\sigma_y + 68.95) \frac{t}{D} \frac{1 - \alpha(d/t)}{1 - \alpha(d/t)/M} \quad (4)$$

where α is the factor used to differentiate between short and long defects,

$$\alpha = \begin{cases} 0.85, & \text{for } \frac{L^2}{Dt} \leq 20 \\ 1 - 0.15 \frac{64 \times 10^6}{\left(\frac{L}{\sqrt{Dt}}\right)^{12}}, & \text{for } \frac{L^2}{Dt} > 20 \end{cases} \quad (5)$$

2.1.5. DNV RP-F101

DNV (DET NORSCHE VERITAS) and BG Technology collaborated to develop the DNV RP-F101 standard, which is based on extensive databases of burst tests and over 400 FEM simulations for corroded pipelines. The equation for calculating the failure pressure of corroded pipelines with a simplified rectangular defect under internal pressure is provided as follows ([“DNV-RP-F101 Corroded pipelines,” 2015](#)),

$$P_f = 1.05 \frac{2t}{D - t} \sigma_u \left(\frac{1 - (d/t)}{1 - (d/t)/M} \right) \quad (6)$$

2.1.6. CSA Z662

The CSA developed a corrosion assessment code that is based on the Shell 92 pressure criterion for both high-grade and low-grade steels. The prediction of failure pressure for corroded pipelines, leading to plastic

collapse, can be achieved using the following equation (CSA, Z662:19, Oil and gas pipeline systems, 2019),

$$P_f = 2 \frac{t}{D} \sigma_f \left(\frac{1 - (d/t)}{1 - (d/t)/M} \right) \quad (7)$$

where σ_f represents the yield strength of low-grade and high-grade steels,

$$\sigma_f = \begin{cases} 1.15\sigma_y, \text{for } \sigma_y \leq 241 \text{ MPa} \\ 0.9\sigma_u, \text{for } \sigma_y > 241 \text{ MPa} \end{cases} \quad (8)$$

2.1.7. FITNET FSS

This formulation, developed by the European Fitness for Service Network, aims to assess the structural integrity of pipelines using a combination of full-scale burst tests and FEM results. The failure pressure for rectangular defects can be calculated using the following equation (Fitness-for-Service, FFS-2021, 2022):

$$P_f = \left(\frac{1}{2} \right)^{65/\sigma_y} \frac{2t}{(D-t)} \sigma_u \left(\frac{1 - (d/t)}{1 - (d/t)/M} \right) \quad (9)$$

2.2. Models based on Buckingham's π theorem

Buckingham's π theorem is a mathematical approach that utilizes dimensionless influencing parameters to predict the quantity of interest. Netto et al. introduced an empirical equation to estimate the failure pressure of pipelines with a single defect based on six full-scale burst tests and a set of nonlinear FEM results. The relationship between several nondimensional variables was investigated, and an iterative process was employed to determine the optimal failure pressure. The expression for this model is provided as (Netto et al., 2005),

$$P_f = 2.2 \frac{t}{D} \sigma_y \left[1 - 0.9435 \left(\frac{d}{t} \right)^{1.6} \left(\frac{L}{D} \right)^{0.4} \right] \text{ for } 0.1 \leq \frac{d}{t} \leq 0.85 \text{ and } \frac{l}{D} \leq 1.5 \quad (10)$$

2.3. Models based on Pipe Corrosion Criterion

2.3.1. PCORRC

The PCORRC approach, developed by Stephens and Leis at Battelle, is based on a series of FEM results using PCORR, a PC-based finite element model that estimates the remaining strength of corrosion defects. This approach is primarily utilized to predict the failure pressure of blunt corrosion pipelines characterized by moderate to high toughness, which fail due to a plastic collapse mechanism. The expression for this model is given as (Stephens and Leis, 2000),

$$P_f = 2 \frac{t}{D} \sigma_u \left\{ 1 - \frac{d}{t} \left[1 - e^{\frac{-0.157L}{D(t-d)/2}} \right] \right\} \quad (11)$$

2.3.2. Modified PCORRC

Due to its limitations in handling low-toughness pipelines and pipelines operating below the ductile-to-brittle transition temperature,

the PCORRC approach required further calibration. To address this issue, Yeom et al. conducted full-scale experimental tests and utilized a set of three-dimensional FEM results specifically for X70 corroded pipelines. They recalibrated the PCORRC model, resulting in an improved version for predicting the failure pressure of such pipelines (Yeom et al., 2015a),

$$P_f = 1.8 \frac{t}{D} \sigma_u \left\{ 1 - \frac{d}{t} \left[1 - e^{\frac{-0.224L}{D(t-d)/2}} \right] \right\} \quad (12)$$

2.4. Models based on other approaches

2.4.1. RAM PIPE REQUAL

The RAM PIPE REQUAL method was developed as a comprehensive engineering approach for risk assessment and management specifically designed for the reassessment and requalification of marine pipeline systems. This approach does not consider the length of the corrosion defect due to the inherent difficulty of obtaining such information for uninstrumented pipelines. The estimated failure pressure can be determined using the following expression (Bea, 1999),

$$P_f = \frac{2.2(t-d)\sigma_u}{(D-t) \left(1 + 2\sqrt{2\frac{d}{D}} \right)} \quad (13)$$

2.4.2. Choi

Choi et al. conducted an extensive series of full-scale experimental tests on the X65 pipeline, incorporating different types of machined pits. Additionally, the authors conducted numerous FEM simulations to establish an appropriate failure criterion and the failure of the pipeline was attributed to plastic collapse. A regression analysis was employed to derive an empirical expression, which is provided as follows (Choi et al., 2003),

$$P_f = \begin{cases} 0.9\sigma_u \frac{2t}{D} \left[C_0 + C_1 \frac{L}{\sqrt{Dt}} + C_2 \left(\frac{L}{Dt} \right)^2 \right], \text{ for } \frac{L^2}{Dt} \leq 36 \\ \sigma_u \frac{2t}{D} \left[C_3 + C_4 \frac{L}{\sqrt{Dt}} \right], \text{ for } \frac{L^2}{Dt} > 36 \end{cases} \quad (14)$$

where coefficients $C_0 = 0.06(d/t)^2 - 0.1035(d/t) + 1$, $C_1 = -0.6913(d/t)^2 + 0.4548(d/t) - 0.1477$, $C_2 = 0.1163(d/t)^2 - 0.1053(d/t) + 0.0292$, $C_3 = -0.9847(d/t) + 1.1101$, and $C_4 = 0.0071(d/t) - 0.0126$.

2.4.3. CUP

Shuai et al. conducted a study using FEM implemented in ABAQUS software to examine the failure characteristics of corroded pipelines. They established the failure criterion as the Von Mises stress reaching the ultimate tensile strength and compared them with the results of 14 sets of full-scale burst tests. Subsequently, they developed a failure pressure prediction model called CUP by fitting the calculated results (Shuai et al., 2017),

$$P_f = 2 \frac{t}{D} \sigma_u \left\{ 1 - \frac{d}{t} \left[1 - \left(0.1075 \left(1 - \left(\frac{w}{\pi D} \right)^2 \right)^6 + 0.8925 e^{\frac{-0.4103L}{\sqrt{Dt}}} \right) \left(1 - \frac{d}{t} \right)^{0.2504} \right] \right\} \quad (15)$$

Table 1 provides an overview of the Folas bulging factors utilized in various models, along with the limitations encountered during their development. It is evident that none of the existing models encompass the entire range of low to high-strength pipelines. Additionally, these models are designed for different types of defect shapes and may yield overly conservative results. Consequently, this can result in unnecessary allocation of resources towards inspection, repair, and maintenance activities.

3. Methodology

Fig. 2 illustrates the framework of the proposed methodology for modeling the failure pressure of corroded pipelines. The subsequent sections elaborate on the specifics of the ML models and the SHAP algorithm.

3.1. ML algorithms

3.1.1. ANN

ANN is a computational model widely employed, inspired by the structure and functioning of biological brains. It comprises interconnected units known as artificial neurons that process and transmit signals through weighted connections. Each neuron's output is computed using a non-linear function applied to the sum of its inputs. Additionally, neurons can possess thresholds, activating and transmitting signals only when the aggregated signal surpasses a specific threshold. Mathematically, an artificial neuron in an ANN can be represented as the weighted sum of inputs, with an activation function applied to it, as expressed in equation (Bishop, 2006),

$$y = f \left(\sum_{i=1}^n w_i \bullet x_i + b \right) \quad (16)$$

where y represents the output of the neuron, f is the activation function, w_i is the weight associated with the i th input x_i , and b is the bias term.

3.1.2. SVR

SVR, a statistical ML technique, is a regression method inspired by SVM. Introduced by Vapnik et al. (Vapnik, 1995), SVR employs SVM principles to estimate the relationship between input variables and a continuous target variable. By utilizing kernel functions, SVR effectively handles non-linear associations and seeks to identify a regression function that minimizes the error while adhering to a specified tolerance margin. The optimization procedure in SVR involves identifying support vectors and determining their corresponding weights using Lagrange multipliers. The prediction is dependent on these support vectors and can be mathematically represented as,

$$y = \sum_{i=1}^n (\alpha - \alpha_i^*) \bullet K(x_i, x) + b \quad (17)$$

where α and α_i^* are Lagrange multipliers, x is the input data point for which the prediction is being made, and K is the kernel function.

3.1.3. KNN

K-Nearest Neighbors (KNN), originally conceived by Evelyn Fix and Joseph Hodges in 1951 and later expanded by Thomas Cover (Fix and Hodges, 1989), is a widely used non-parametric supervised learning method for classification and regression tasks. KNN determines the output by considering the average value of the k nearest training examples from a dataset, with the option to weight the contributions of neighbors, especially those in close proximity. KNN's notable feature is its sensitivity to the local data structure, devoid of any assumptions about data distribution. However, KNN can be computationally and

memory-intensive, particularly with large datasets, and it is susceptible to the curse of dimensionality. Employing preprocessing techniques such as normalization can help mitigate these challenges.

3.1.4. DT

The decision tree, a versatile supervised learning algorithm used for tasks like classification and regression, constructs a tree-like structure with nodes representing attribute tests, branches indicating outcomes, and leaves containing class labels or responses. It recursively splits training data based on attributes until a specified stopping criterion is reached (Quinlan, 1986), selecting attributes during training to maximize information gain or reduce impurity. Decision trees are capable of predicting both nominal and numeric responses, making them adaptable for various tasks. They provide a nonparametric approach to data partitioning and simplify complex data patterns into interpretable rules, laying the foundation for the development of various ensemble methods discussed in subsequent sections.

3.1.5. RF

RF is an ensemble learning method that mitigates the overfitting problem typically encountered with decision trees. It addresses this issue by creating a multitude of decision trees during training for tasks such as classification and regression. RF incorporates the random subspace method and the concept of bagging to generate a collection of decision trees with controlled variance. By introducing randomness during the construction process, RF reduces the variance of the estimator and combines diverse trees, leading to enhanced accuracy. To obtain the final prediction for a new sample x , the predictions from all individual learners are averaged (Breiman, 2001),

$$\widehat{T}_{rf}(x) = \frac{1}{N} \sum_{i=1}^N \widehat{T}_i(x) \quad (18)$$

where \widehat{T}_i are trained individual learners using the randomly selected samples, N is the number of individual learners and $\widehat{T}_{rf}(x)$ is the final prediction.

3.1.6. AdaBoost

AdaBoost, introduced by Freund and Schapire (Freund and Schapire, 1995), is a renowned boosting algorithm known for its proficiency in enhancing the performance of weak learners, particularly small decision trees. This iterative approach involves training these weak learners on adjusted versions of the training data and then combining their predictions using weighted majority voting or summation to yield the final prediction. In each iteration, AdaBoost adapts sample weights, prioritizing instances previously misclassified while diminishing the weights of correctly classified ones. This adaptability steers subsequent weak learners towards challenging examples. AdaBoost is esteemed for its ability to boost the performance of other learning algorithms, its resistance to overfitting, and its computational efficiency, simplicity, and applicability across diverse learning tasks.

3.1.7. GBDT

GBDT is a robust ML method that combines weak prediction models, typically decision trees, into a powerful ensemble. GBDT iteratively trains models to minimize the gradient of a differentiable loss function with respect to the ensemble's predictions, stopping when predefined criteria are met (Friedman, 2001). GBDT often outperforms RF and is popularized by implementations like XGBoost. To enhance efficiency and scalability, techniques like Gradient-based One-Side Sampling (GOSS) and Exclusive Feature Bundling (EFB) have been introduced. GOSS optimizes data size by excluding instances with small gradients, improving information gain estimation accuracy, while EFB reduces features without compromising split point accuracy. Random subsampling can further improve accuracy and reduce computational costs.

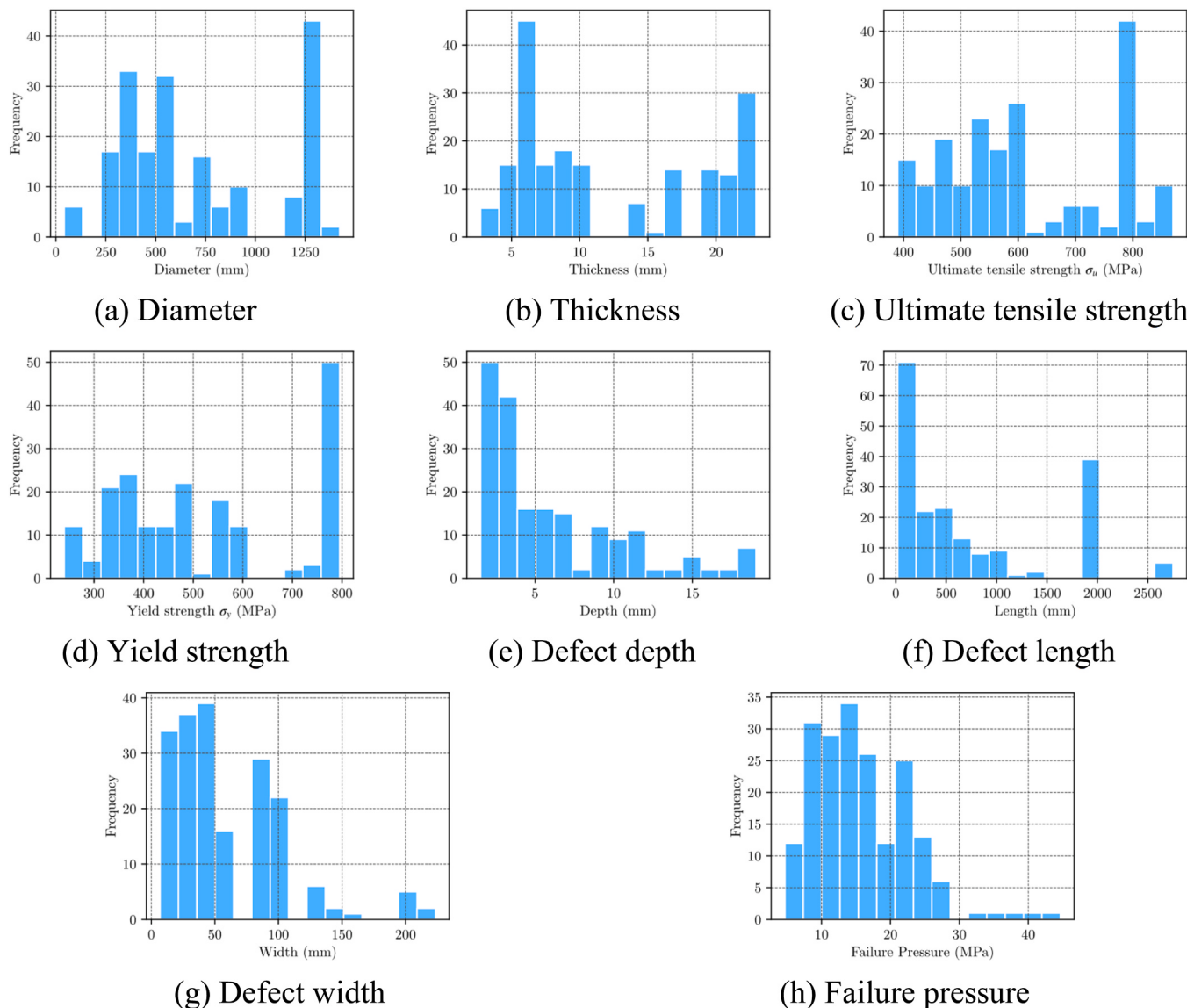


Fig. 3. Histograms of the eight parameters in the database.

3.2. SHAP

To gain further insight into the outputs of the ML models developed in this study, the SHAP method is employed to elucidate the impact of input features on the failure pressure. SHAP draws inspiration from cooperative game theory and utilizes the Shapley value explanation as an additive feature attribution technique (Lundberg and Lee, 2017),

$$g(\mathbf{z}') = \phi_0 + \sum_{i=1}^M \phi_i x'_i \quad (19)$$

where g is the explanation model, \mathbf{z}' is the simplified input feature vector, M is the number of input features and ϕ_i is the feature attribution for the i th feature.

The SHAP value possesses three desirable properties, namely local accuracy, missingness, and consistency. These properties dictate that for a given simplified input mapping, there exists a single additive feature attribution method that satisfies all three properties. This unique model can be represented as (Lundberg and Lee, 2017),

$$\phi_i(f, x) = \sum_{\mathbf{z} \subseteq \mathbf{x}} \frac{|\mathbf{z}'|!(M - |\mathbf{z}'| - 1)!}{M!} [f_x(\mathbf{z}') - f_x(\mathbf{z}' \setminus i)] \quad (20)$$

where $|\mathbf{z}'|$ is the number of non-zero entries in \mathbf{z}' , and $\mathbf{z}' \subseteq \mathbf{x}'$ represents all \mathbf{z}' vectors where the non-zero entries are a subset of the non-zero entries in \mathbf{x}' .

The computation of SHAP values as described in Eq. (20) can be highly complex due to the numerous combinations of feature subsets, which is generally an NP-hard problem. To address this, several approximations have been proposed, such as Kernel SHAP and TreeSHAP (Lundberg et al., 2020). Once the SHAP values are obtained, they can be used to indicate the contribution of each feature in shifting the model's expected output towards the output of a specific prediction. It is important to note that the sum of SHAP values for all input features equals the difference between the expected model output and the current prediction. By aggregating the impacts of each feature across all instances, a global measure of feature importance can be derived. For more detailed information about SHAP values, please refer to the papers (Lundberg et al., 2020; Lundberg and Lee, 2017).

3.3. Evaluation metrics

The predicted failure pressure of the models will be compared against the true values, and various commonly used quantitative metrics

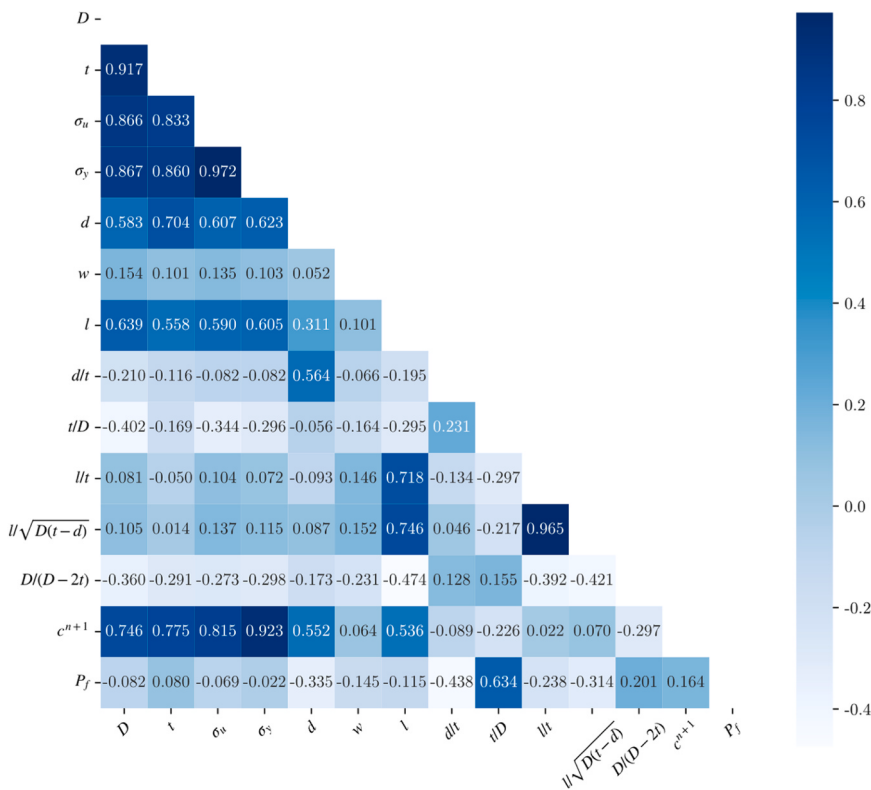


Fig. 4. Correlation matrix heatmap for input parameters.

will be employed to evaluate the performance of each model. These metrics are defined as follows (Kendall et al., 1994; Hyndman and Koehler, 2006),

- Mean absolute error (MAE)

$$\text{MAE} = \frac{1}{N} \sum_{i=1}^N |\hat{P}_{fi} - P_{fi}| \quad (21)$$

- Mean absolute percentage error (MAPE),

$$\text{MAPE} = \frac{1}{N} \sum_{i=1}^N \frac{|\hat{P}_{fi} - P_{fi}|}{P_{fi}} \quad (22)$$

- Root mean square error (RMSE)

$$\text{RMSE} = \sqrt{\frac{1}{N} \sum_{i=1}^N (\hat{P}_{fi} - P_{fi})^2} \quad (23)$$

- Coefficient of determination R -squared (R^2)

$$R^2 = 1 - \frac{\sum_{i=1}^N (\hat{P}_{fi} - P_{fi})^2}{\sum_{i=1}^N (\hat{P}_{fi} - \bar{P}_f)^2} \quad (24)$$

where \hat{P}_{fi} and P_{fi} are the predicted and actual failure pressures, respectively, \bar{P}_f is the average value of the actual failure pressures and N is the number of predictions.

4. Model development and results

4.1. Data collection

In this study, the prediction models are developed using data sourced from published literature (Benjamin et al., 2005, 2000; Chauhan and Crossley, 2009; Chen et al., 1998; Cronin and Pick, 2000; Diniz et al., 2006; Freire et al., 2006; Kim Yeong-Pyo et al., 2002; Liu et al., 2009; Ma et al., 2013; Mannucci et al., 2002; Mok et al., 1991; Netto et al., 2005; Oh et al., 2007; S.Cronin, 2000; Shuai et al., 2017; Souza et al., 2007; Yeom et al., 2015c), which exclusively consists of full-scale experimental tests. It should be noted that there may be some overlap in the experimental data included in these studies. To ensure the exclusion of duplicate data, a thorough inspection is conducted. The dataset comprises a total of 193 sets of samples, each consisting of eight parameters: pipe diameter, pipe thickness, ultimate tensile strength, yield strength, defect depth, length, width, and recorded failure pressure for each pipeline. In certain studies, the defect width was not recorded, and thus it is assumed to be $0.05\pi D$ based on the assumption made by Choi et al. and Kere & Huang (Choi et al., 2003; Kere and Huang, 2022). The statistical distributions of these parameters are presented in Fig. 3.

The existing empirical models have been found applicable to different strength categories, namely low, low to medium, or medium to high strength pipelines. However, considering the increasing use and anticipated widespread adoption of high-strength steel in the near future, it becomes imperative to develop a prediction model that covers all grades of steel pipelines. To achieve this, the database encompasses a diverse range of steel grades, including X42, X46, X52, X56, X60, X65, X80, X100, and X120. It is worth noting that the exclusion of FEM results from the dataset, which were utilized in other studies (Lu et al., 2021a; Phan and Duong, 2021; Su et al., 2021), does reduce the dataset's size. However, as demonstrated in subsequent sections, the methodology proposed in this study yields quite promising results.

4.2. Feature engineering

Typically, the pipe and defect parameters can be directly utilized in the development of prediction models, as demonstrated in previous studies (Chen et al., 2023; Oh et al., 2020; Zhang et al., 2023). These parameters have been identified as potential contributors to pipeline failure. However, insightful observations have revealed intriguing interactions among these parameters. For instance, it has been noted that pipelines with exceptionally thick walls exhibit distinct patterns regarding the influence of yield strength on failure pressure (Kere and Huang, 2022). Moreover, it is recognized that the failure of corroded gas pipelines under internal pressure constitutes a complex phenomenon. The precise mechanisms of failure have yet to be fully elucidated and cannot be adequately captured by conventional parameters pertaining to the pipeline and its corrosion defects alone. Consequently, it becomes crucial to incorporate additional essentials associated with the underlying failure process of corroded pipelines. This augmentation of information will not only enrich the understanding of the failure behavior of corroded gas pipelines, but also enhance the performance of the developed models.

First, several features with meaningful physical interpretations are derived based on existing empirical models. Upon examining the empirical formulas of Eqs. (1) to (15) and the Folias bulging factors presented in Table 1, it becomes evident that the degree of corrosion relative to pipe size may significantly influence the residual strength of corroded gas pipelines. This relationship can be quantitatively described by the following dimensionless parameters: 1) the ratio of defect depth to pipe wall thickness (d/t), 2) the ratio of defect length to pipe wall thickness (l/t), 3) the ratio of pipe wall thickness to pipe diameter (t/D), and 4) a ratio involving defect length, the square root of the product of pipe diameter, and the difference between pipe wall thickness and defect depth ($L/\sqrt{D(t-d)}$) is introduced to identify the presence of long or short corrosion defects.

Then, the failure pressure of a corroded gas pipeline can generally be formulated in terms of the previously described dimensionless parameters and a reference pressure (Keshtegar and El Amine Ben Seghier, 2018; Zhu, 2021)

$$P_b = P_r f\left(\frac{d}{t}, \frac{l}{t}, \dots\right) \quad (25)$$

where P_r represents the reference failure pressure for the defect-free pipe, and $f(\bullet)$ is a modification coefficient that incorporates the influence of the corrosion defect.

In the case of defect-free pipes, many empirical models for predicting burst pressure have been formulated and can be expressed as

$$P_r = C_0 g(\sigma_u, \sigma_y) \ln(D/D_i) \quad (26)$$

where C_0 is a coefficient, $g(\bullet)$ denotes a function dependent on the ultimate tensile strength and yield strength of the pipe's material, and D_i is the internal diameter of the pipe.

As posited in the introduction, the strain hardening effect influences the residual strength of corroded gas pipelines. To account for the plastic flow effect, the flow theory of plasticity, applied in the context of large deformations, has been utilized to describe the plastic collapse of corroded pipelines, with the resulting expressions for burst pressure presented as follows (Zhu, 2023)

$$P_r = C_{sh}^{n+1} g(\sigma_u, \sigma_y) \quad (27)$$

where C_{sh} is the strain hardening coefficient with regard to the various yield criteria, and n is the strain hardening exponent.

Drawing upon the physical laws and the insights gleaned from the above analysis of the failure behavior of corroded gas pipelines, this study proposes the addition of two features: 1) the logarithm of the ratio of the pipeline's external diameter to its internal diameter $\ln(D/D_i)$, and

Table 2

Grid search settings and results for ML algorithms.

Model	Hyperparameter	Range	Optimal value
ANN	1) Hidden layers 2) Nodes in hidden layers 3) Activation function	[1:5], [10:10:100], [logistic, tanh, relu]	3, 50, relu
SVR	1) Regularization parameter 2) Kernel coefficient	[1×10 ⁻⁴ :1×10 ⁴], [1×10 ⁻³ :1×10 ³]	1000, 0.1
KNN	1) Number of neighbors 2) Weight function	[1:10], [uniform, distance]	2, uniform
DT	1) Maximum depth 2) Minimum samples for split 3) Minimum number at leaf node	[2:2:12], [2:5], [1:3]	10, 2, 3
RF	1) Number of trees 2) Maximum depth 3) Minimum samples for split 4) Minimum number at leaf node 5) Number of randomly features	[100:500], [2:2:12], [2:5], [1:3], [sqrt, log2, all]	200, 10, 2, 1, log2
AdaBoost	1) Number of trees 2) Maximum depth 3) Minimum samples for split 4) Minimum number at leaf node	[100:500], [2:2:12], [2:5], [1:3]	200, 8, 2, 1
GBDT	1) Number of trees 2) Maximum depth 3) Minimum samples for split 4) Minimum samples of leaf node 5) Minimum decrease of impurity	[100:500], [2:2:12], [2:5], [1:3], [0:1×10 ³]	200, 8, 2, 1, 0.1

2) the strain hardening coefficient, denoted as C_{sh}^{n+1} in terms of von Mises flow theory. Consequently, the feature vector integrates seven traditional size-related attributes of pipes and defects, four dimensionless characteristics, and two additional features grounded in physical insights. Fig. 4 displays the correlation matrix for these features within the vector. Notably, the wall thickness to diameter ratio (t/D) demonstrates the most significant correlation with failure pressure. Additionally, several other parameters including d/t , $L/\sqrt{D(t-d)}$ and d show substantial correlations with failure pressure as well, highlighting strong intercorrelations among pipe parameters. In summary, a total of thirteen features will be utilized in this study for the development of prediction models.

Before utilizing the parameters for the development of prediction models, it is common practice to normalize the data. This normalization step aims to eliminate magnitude differences among the input parameters and enhance the convergence and performance of the models. The input parameters are normalized using the following method,

$$x^* = \frac{x - x_{\min}}{x_{\max} - x_{\min}} \quad (28)$$

where x_{\max} and x_{\min} denote the maximum and minimum values of the data respectively.

4.3. Model development

The entire dataset is prepared and randomly divided into training and testing sets, following an 8:2 ratio. Specifically, 154 samples are used for developing the prediction models, while the remaining 39

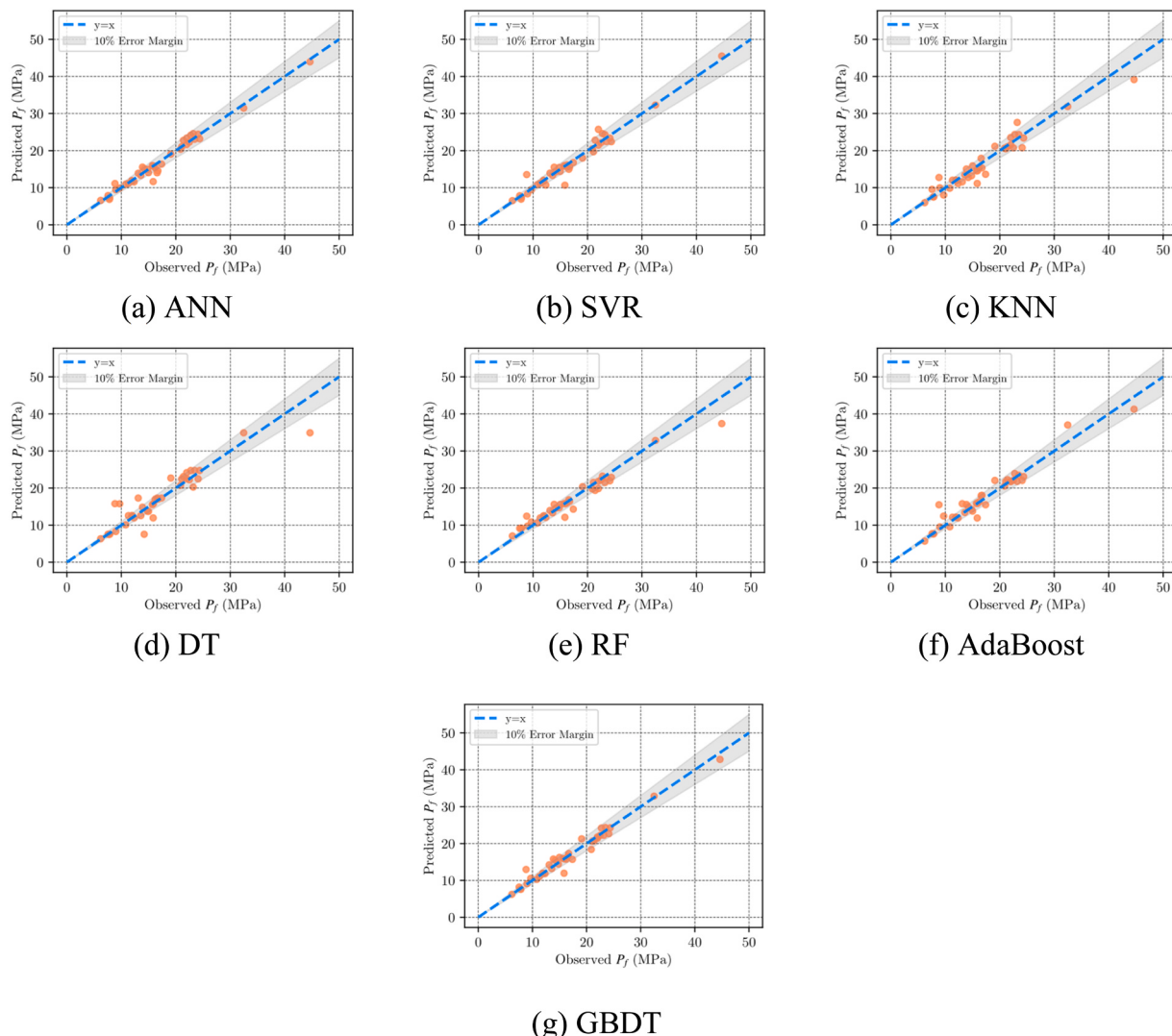


Fig. 5. Failure pressure of corroded pipelines predicted by (a) ANN, (b) SVR, (c) KNN, (d) DT, (e) RF, (f) AdaBoost and (g) GBDT.

Table 3
Performance evaluation of developed prediction models.

Model	MAE	MAPE	RMSE	R ²
ANN	0.842	0.056	1.188	0.974
SVR	1.006	0.067	1.540	0.956
KNN	1.485	0.094	1.993	0.927
DT	1.781	0.115	2.834	0.852
RF	1.187	0.078	1.799	0.941
AdaBoost	1.263	0.084	1.909	0.933
GBDT	0.891	0.059	1.317	0.968

samples are reserved for evaluating the model performance. Given the importance of hyperparameters in achieving high-performance models, this study adopts a combination of grid search and k-fold cross-validation techniques to determine the optimal hyperparameters for all ML models (Bishop, 2006). For the SVR model, the radial basis function (RBF) is selected as the kernel function. DT are chosen as the weak learners for ensemble methods. The potential value ranges for the model parameters are determined based on previous experience and literature. Table 2 provides the defined value ranges for the model parameters, represented as grids, as well as the determined hyperparameters for all models through 10-fold cross-validation.

Table 4
Comparative performance of recent studies for residual strength estimation.

Source	Feature set	Algorithm	MAE	MAPE	RMSE	R ²
(Phan and Dhar, 2021)	D, t, σ_u , d, l	SVR	1.415	0.078	2.337	0.899
(Su et al., 2021)	D, t, σ_u , d, w, l	DNN	1.210	0.079	1.714	0.946
(Chen et al., 2023)	D, t, d, l, Grade	ANN	1.197	0.080	1.732	0.944
(Ma et al., 2023a)	D, t, σ_u , σ_y , d, w, l, Grade, σ_y/σ_u , d/t, w/D, t/D, L/ $\sqrt{D(t-d)}$, $\pi(dl+dw+wl/2)/3$	LightGBM	1.337	0.087	1.874	0.935
Present study	D, t, σ_u , σ_y , d, w, l, d/t, t/D, L/t	ANN	1.316	0.085	1.749	0.943
	D, t, σ_u , σ_y , d, w, l, d/t, t/D, L/t, L/ $\sqrt{D(t-d)}$, D/(D _l), C _{sh} ⁿ⁺¹	ANN	0.842	0.056	1.188	0.974

Table 5

Performance comparison between the ML models and existing empirical models.

Model	MAE	MAPE	RMSE	R^2
ASME B31G	4.005	0.258	5.131	0.515
Modified ASME B31G	3.038	0.197	4.077	0.694
SHELL-92	3.890	0.234	5.050	0.531
RPA	3.098	0.196	4.155	0.682
DNV RP-F101	2.131	0.136	2.924	0.843
CSA Z662-07	3.654	0.223	4.763	0.582
FITNET FSS	3.637	0.221	4.887	0.560
Netto	3.626	0.210	5.113	0.519
PCORRC	2.258	0.146	3.067	0.827
Modified PCORRC	3.776	0.231	4.813	0.573
RAM PIPE REQUAL	6.460	0.382	8.170	-0.229
Choi	2.632	0.156	3.333	0.795
CUP	2.186	0.136	3.191	0.812
ANN	0.842	0.056	1.188	0.974

4.4. Prediction results

The performance evaluation of the prediction models is conducted using the testing dataset, where predicted failure pressures are compared to actual experimental values. These evaluations, illustrated in Fig. 5, reveal that all models closely align with the ideal line ($y = x$), indicating favorable results. Further assessment is carried out using various metrics, summarized in Table 3. Remarkably, ANN demonstrates the best performance with metrics of $MAE = 0.842$, $MAPE = 5.60\%$, $RMSE = 1.188$, and $R^2 = 0.974$, while DT yields less favorable results. Other models, including GBDT, SVR, RF, and AdaBoost, also yield commendable predictive results. The majority of failure pressures fall below 25 MPa, with a few outliers linked to small pipeline sizes and shallow, short defect lengths. Nevertheless, most prediction models effectively estimate failure pressures for these cases. As the dataset spans various steel grades, these results highlight the models' suitability for engineering applications. However, it's noted that further improvements can be achieved with an expanded dataset. Thus, collecting additional full-scale experimental or field data is recommended to enhance the applicability and performance of the developed models.

To demonstrate the efficacy of the proposed methodology, this study compares it with methodologies from existing literature, employing them as baseline performance. To ensure a fair comparison and derive meaningful reference metrics, the feature sets, model architectures, and hyperparameters are aligned with those reported in the referred studies. In addition to the above analysis, the feature set was modified to exclude three variables: $L/\sqrt{D(t-d)}$, $D/(D_t)$, and C_{sh}^{t+1} , investigating the influence on the performance of the prediction model. Table 4 details the features, models, and performance measures from the pertinent research. The results indicate that the models developed in the current study outperform the baseline performance in terms of MAE, MAPE, RMSE, and R^2 . For models included in Table 3 but not Table 4, a consistent improvement is also observed, underscoring the robustness of the proposed approach. It is also observed that the model, when developed without incorporating the additional features proposed in the current study, exhibits a noticeable decline in performance across all metrics. The results here suggest that the integration of comprehensive feature engineering, which leverages physical insights, enhances the models' predictive accuracy regarding the estimation of remaining strength. The amalgamation of domain knowledge with ML techniques emerges as a key element in advancing predictive analytics within this field.

4.5. Comparison with existing empirical models

In comparing the performance of existing empirical models, as detailed in Section 2, with the developed prediction models, the results summarized in Table 5 and illustrated in Fig. 6 reveal distinct trends. Among the existing empirical models, DNV RP-F101 stands out with the

highest performance, boasting metrics of $MAE = 2.131$, $MAPE = 13.60\%$, $RMSE = 2.924$, and $R^2 = 0.843$, followed closely by CUP and PCORRC, while RAM PIPE REQUAL performs less favorably. Importantly, many of the existing empirical models tend to provide conservative predictions, potentially leading to excessive resource allocation for inspection and maintenance in practical applications. In stark contrast, ML models developed in this study exhibit superior performance. For example, when considering ANN, the metrics MAE, MAPE, and RMSE experience an approximate two-fold reduction, while R^2 shows a significant improvement. Moreover, the ML models excel in predicting "outliers," highlighting their superior capability in forecasting the failure pressure of corroded pipelines. These findings underscore the practical advantages of ML models in this context.

In Fig. 7, a comparison between three superior ML models and three existing empirical models (DNV RP-F101, CUP, and PCORRC) is presented based on the ratio of predicted failure pressure to experimental test results, with mean and standard deviation values provided. Notably, the ANN model exhibits superior performance, demonstrating a mean value close to 1 and the smallest standard deviation of 0.082. It also yields more compact forecasting results, tightly clustered around the desired horizontal unity line, compared with other models. Furthermore, DNV RP-F101 outperforms other existing empirical models. Generally, ML models outperform existing empirical models, evident from their mean values closer to 1 and smaller standard deviations. It is noteworthy that the majority of existing empirical models, except for DNV RP-F101, tend to underestimate it, indicating their conservative nature. These findings underline the effectiveness of the ML models developed in this study for accurate prediction of corroded pipeline failure pressure.

4.6. Model interpretation

ML models are often considered "black box" models, making it challenging to understand the influence of individual factors or parameters on the output and their interactions. To address this issue, SHAP is employed for interpreting the contribution of each parameter to predicted failure pressure. Using GBDT as an example, Fig. 8 presents a SHAP summary plot of the parameters, where the x-axis represents SHAP values, ordered by importance on the y-axis. Pink and blue colors indicate large and small parameter values, respectively. This plot offers insights into the distribution of SHAP values for each feature and their impact on the failure pressure of corroded pipelines. Generally, an increase in values of t/D , $D/(D-2t)$, t , σ_y , and σ_u enhances the capacity against internal pressure, while an increase in values of d/t , d , $L/\sqrt{D(t-d)}$, l/t , and l diminishes this capability, aligning with previous studies (Netto et al., 2005; Zhu, 2021). Although the correlation matrix in Fig. 4 reveals a negative correlation between strength and failure pressure, empirical formulas consistently indicate a positive correlation with pressure. This suggests that while the correlation matrix is useful for selecting input features, it may not provide clear insight into the contribution of each feature to the predictive outcomes. Thus, SHAP provides a comprehensive explanation of parameter contributions to corroded pipeline failure pressure on a global scale, aiding in the interpretability of ML models.

Fig. 9 complements the summary plot presented in Fig. 8 by illustrating a feature dependence plot, which delineates how SHAP values vary with changes in predictor variables. It is evident that there is a significant positive correlation between the ratio t/D and the failure pressure, whereas negative correlations are present for d/t and d with the failure pressure. Specifically, a t/D ratio below 0.02, a d/t ratio exceeding 0.04, or a d value greater than 2 is associated with a marked decrease in the residual strength of corroded gas pipelines. These insights are crucial for optimizing gas pipeline design to enhance resistance to corrosion-induced failure. Additionally, the partial dependence plots in Fig. 9 reveal interaction effects among various features. For

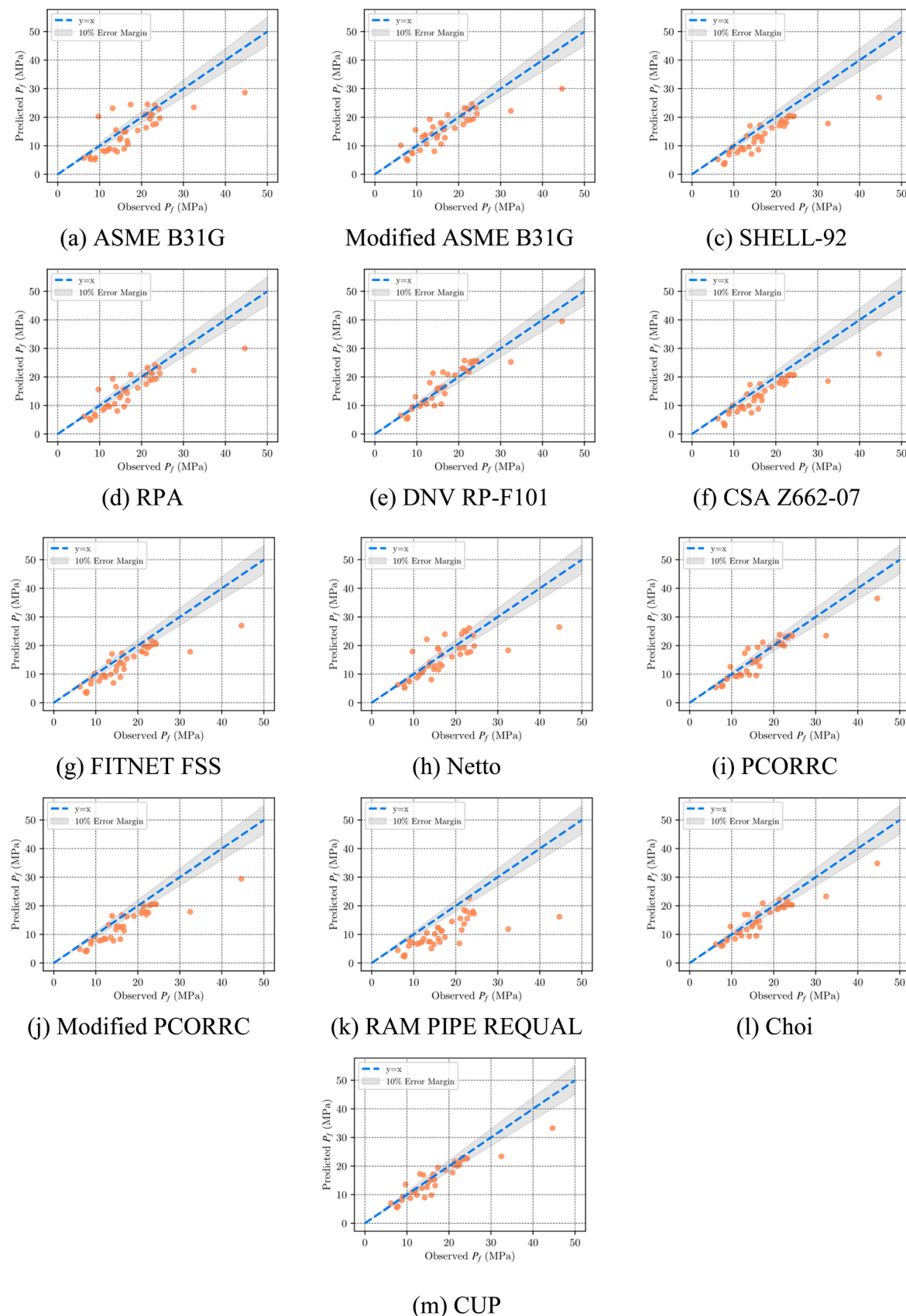


Fig. 6. Failure pressure of corroded pipelines existing empirical models.

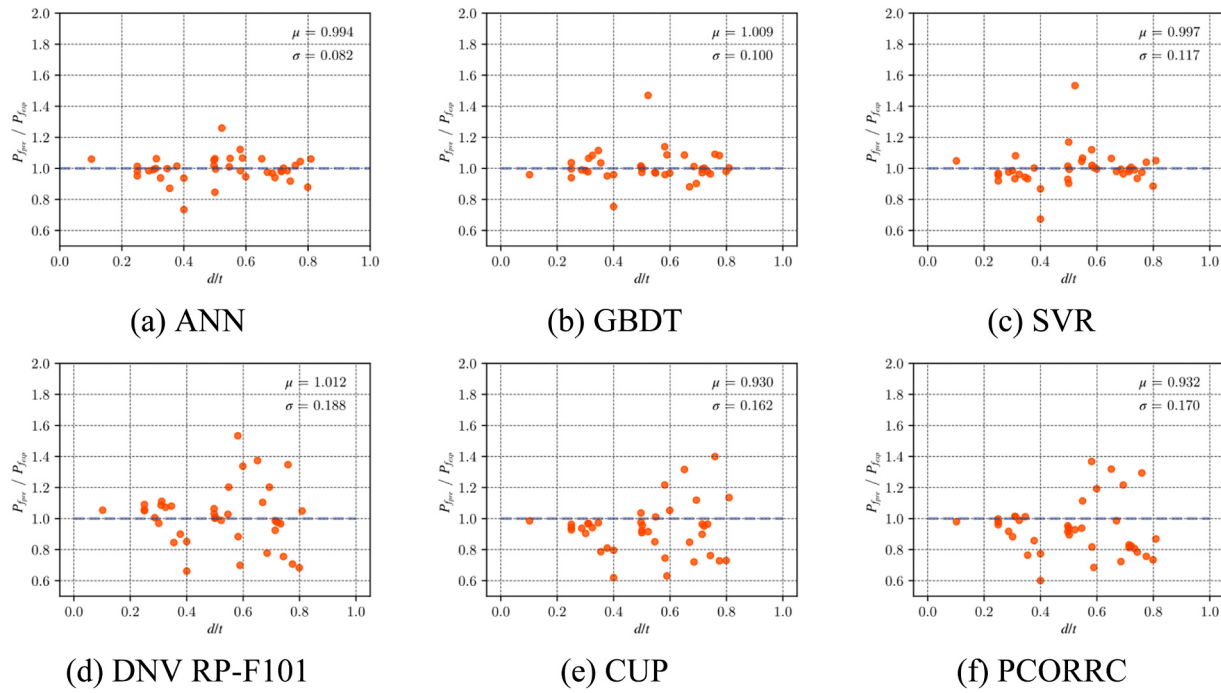


Fig. 7. Ratio of predicted failure pressure against experimental test results with respect to the ratio of defect depth and pipeline thickness.

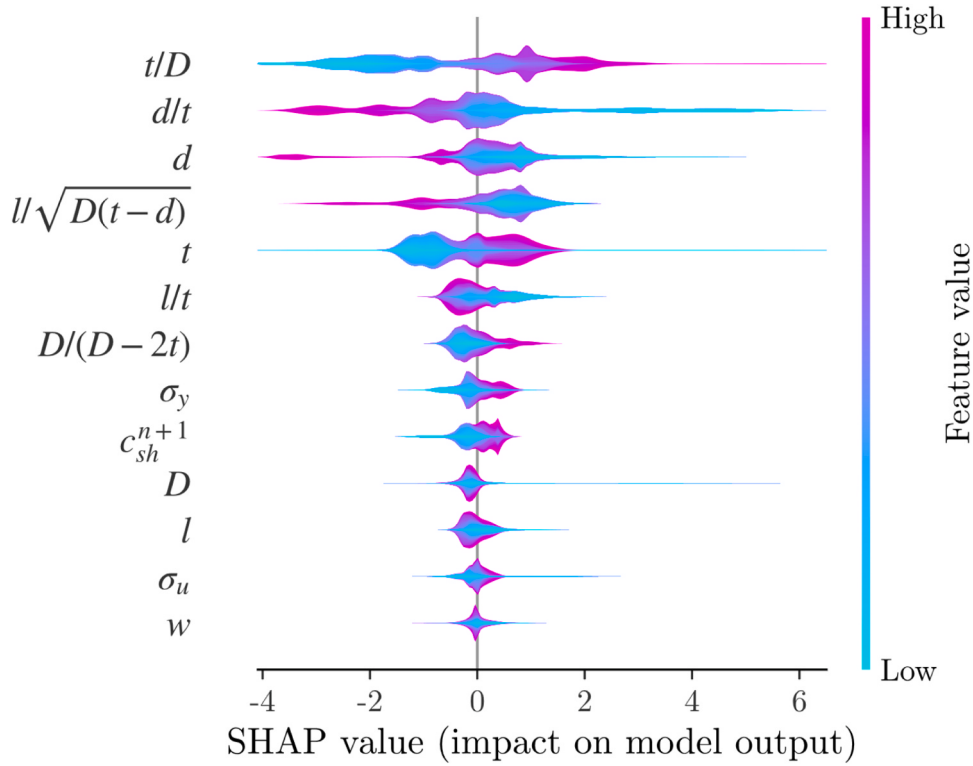


Fig. 8. SHAP summary plot of parameters.

instance, at a fixed t/D and d/t , higher values of $L/\sqrt{D(t-d)}$ and t/d correspond to increased SHAP values, suggesting that such alterations can improve the pipelines' residual strength under specific conditions. The complex interdependencies observed in the feature dependence plot warrant further in-depth theoretical investigation to elucidate the underlying mechanisms. The findings presented here serve as a valuable reference for engineers and researchers in determining the critical

parameters for designing gas pipelines that are more resilient to corrosion-induced failure.

The evaluation of parameters' overall importance on failure pressure involves averaging their impacts across all samples. Fig. 10 (a) illustrates the relative feature importance, with the relative ratio of t/D having the most significant impact, followed by the ratio of d/t , defect depth d and pipe thickness t , in predicting failure pressure. Conversely, material

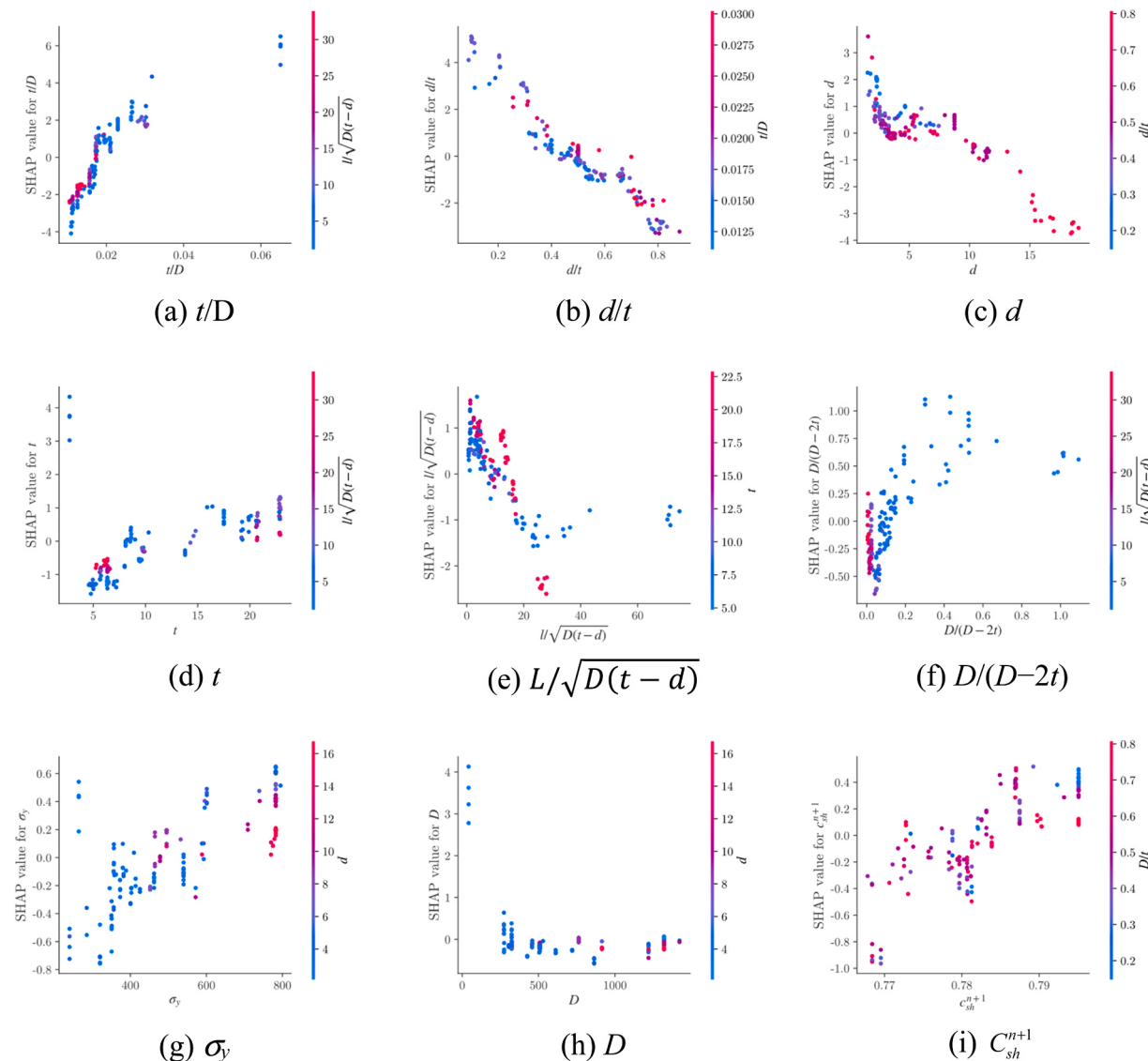


Fig. 9. SHAP feature dependence plot.

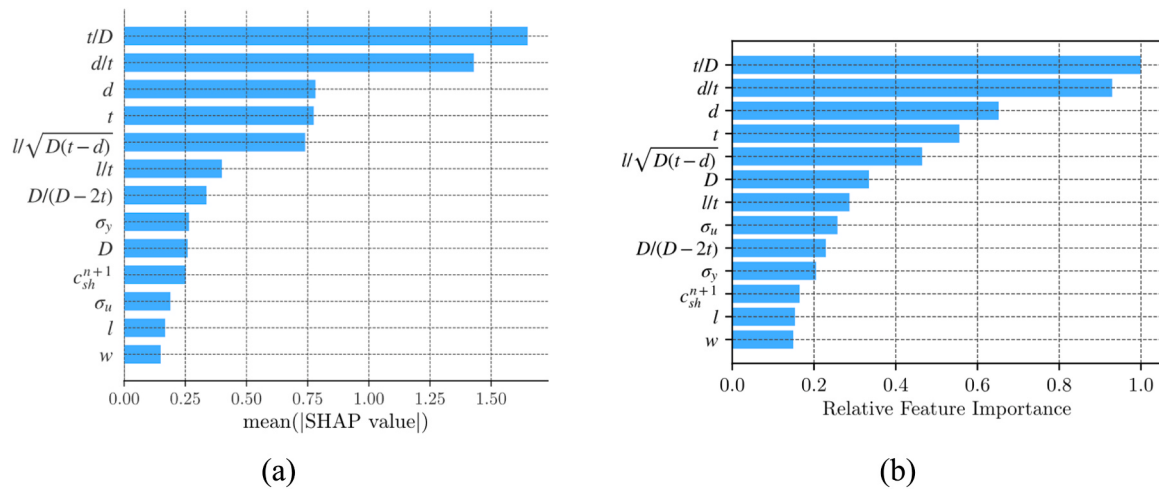


Fig. 10. Feature importance by (a) SHAP, and (b) GBDT.

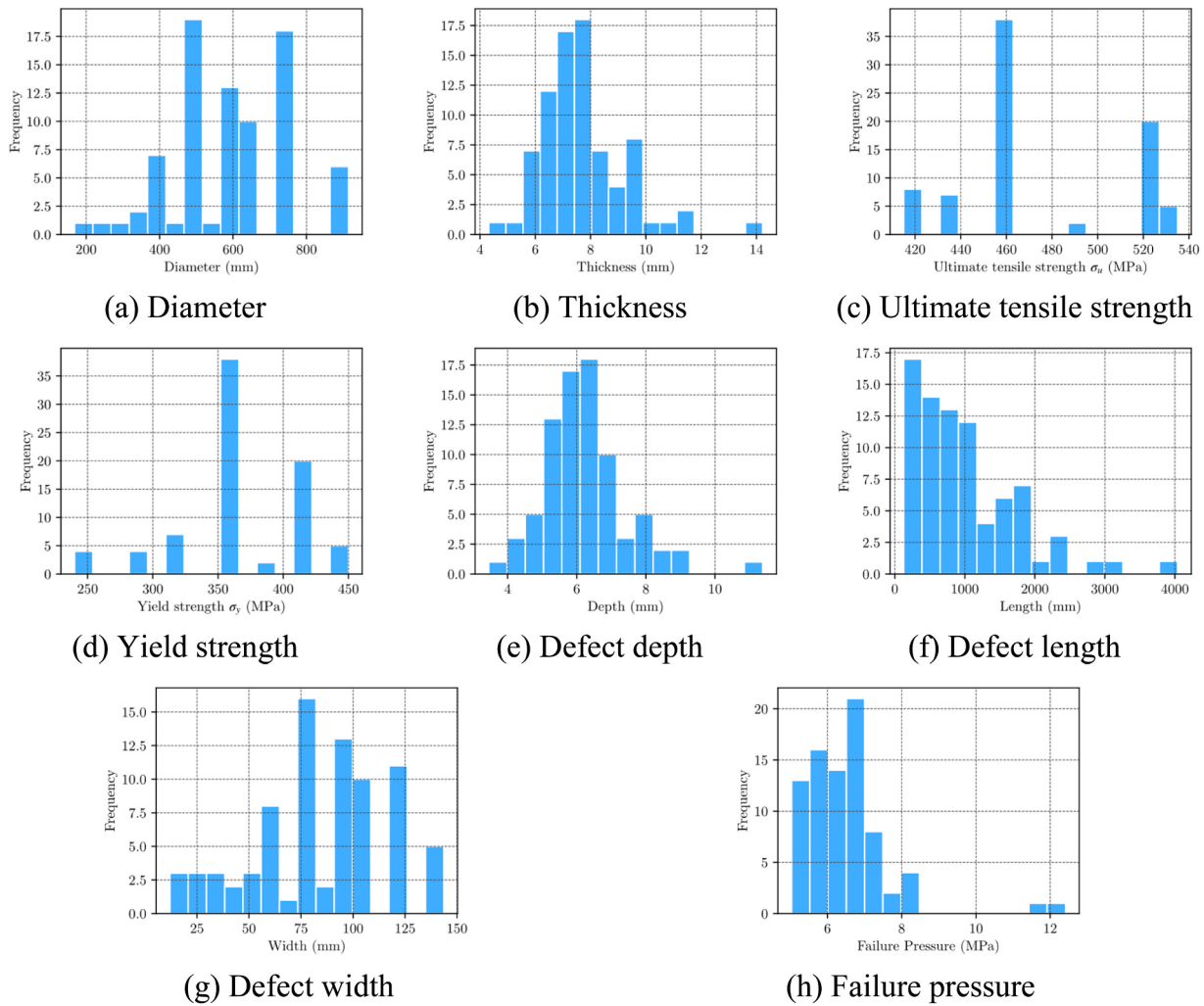


Fig. 11. Histograms of the parameters of incident pipelines in the PHMSA database.

properties, absolute defect length, and width exhibit lesser influence. A comparison in Fig. 10 (b) with GBDT's permutation importance reveals a similar order of importance, where the relative ratio of t/D , d/t , defect depth d and pipe thickness t are the most critical parameters, while parameters w , l , σ_y , and σ_u are considered less important. The findings from SHAP and GBDT feature importance analyses concur that the ratios of t/D and t/d , along with d , are the most significant features. This is corroborated by the feature correlation matrix presented in Fig. 4. Although the pipe thickness exhibits a minimal correlation with failure pressure, it is assigned a relatively high importance value as depicted in Fig. 10.

5. Case study

The existing studies have relied on their own collected data from experimental and numerical simulations for training and validation purposes, without any evaluation using field data. Therefore, it is crucial to assess the applicability of prediction models in real engineering practice. The PHMSA has been amassing comprehensive information on gas pipeline incidents from local operators since 1970. This extensive database encompasses details concerning pipe location, characteristics, incident data and location, inspection history, consequences, and more (PHMSA, 2023). To further investigate the developed prediction models, this study will utilize a portion of this database.

Before conducting database analysis, a thorough data cleaning process is employed to identify suitable samples for examination. The initial

dataset, spanning incidents from 1986 to the present and sourced from PHMSA, encompasses pipeline incidents attributed to various causes, including external force damage, corrosion, material or weld failure, equipment malfunction, and incorrect operation. This study exclusively focuses on incidents related to corrosion, particularly those induced by external corrosion, while excluding plastic pipes and cases with unknown pipe materials. Additionally, incidents lacking critical parameters essential for pipe failure prediction, such as pipe diameter, thickness, strength, and rupture length, are rigorously filtered out. Notably, due to the dataset's nature of previously failed pipelines, data regarding defect depth is unavailable. To facilitate analysis, a defect depth of 0.8 times the pipe thickness is assumed, a common upper limit in existing empirical models. Ultimately, 80 samples are selected for model evaluation. Statistical distributions of pipeline-related factors are depicted in Fig. 11, revealing that the highest steel grade in the dataset is X65, suggesting potential improvements in model performance compared to previous datasets. Furthermore, it is observed that the failure pressures of these pipelines predominantly fall below 10 MPa.

In this comparative analysis, three superior ML models (ANN, GBDT, and SVR) and three previously high-performing existing empirical models (DNV RP-F101, CUP, and PCORRC) are assessed using the PHMSA dataset in Fig. 12. The existing empirical models tend to provide conservative predictions, potentially leading to inefficient resource allocation for inspection and maintenance. Conversely, ML models tend to overestimate failure pressures, introducing a substantial risk, as higher values might erroneously be deemed within safety limits,

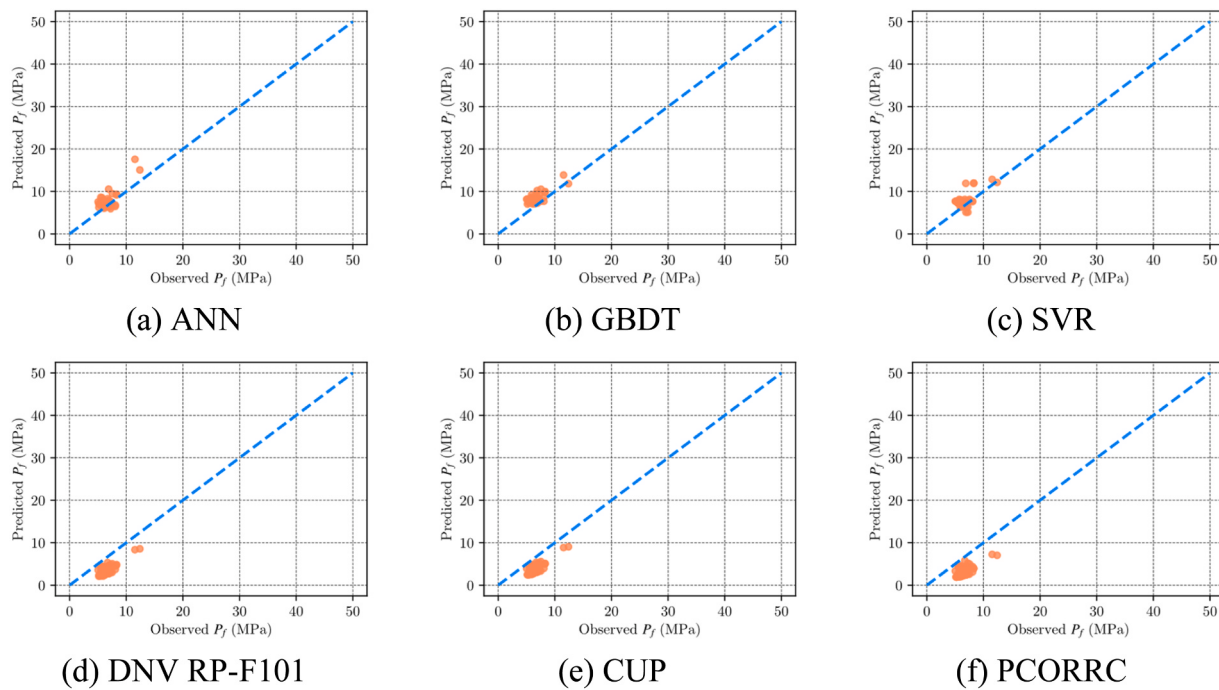


Fig. 12. Comparison of predicted failure pressure of corroded pipelines using ensemble methods and best empirical models on the PHMSA dataset.

Table 6
Comparative performance analysis of ML models and existing empirical models on PHMSA dataset.

Category	Model	MAE	MAPE	RMSE
ML models	ANN	1.158	0.181	1.460
	GBDT	1.320	0.207	1.498
	SVR	1.340	0.217	1.593
Existing empirical models	DNV RP-F101	3.263	0.505	3.345
	CUP	2.961	0.458	3.054
	PCORRC	3.614	0.557	3.729

carrying the potential for severe consequences. Multiple factors contribute to prediction errors, including the need to assume defect depth due to the dataset comprising already failed pipelines and the likelihood of incidents being observed some time after they occur, often resulting in recorded pipeline pressures lower than actual failure pressures. In such scenarios, ML models align more closely with actual values, while existing empirical models exhibit greater deviations. These findings underscore the complexity of predicting corroded pipeline failure pressures and emphasize the importance of careful model selection in practical applications, considering safety implications and resource allocation.

The performance evaluation metrics for the six models, as presented in Fig. 12, are detailed in Table 6. Once again, ANN exhibits the highest performance among all models, achieving metrics of MAE = 1.158, MAPE = 18.1%, and RMSE = 1.460. Notably, MAE and RMSE values are relatively smaller than those in Table 5, while the relative error MAPE remains at a comparable level, which is acceptable given the ML model was tested on a completely new dataset. Among the existing empirical models, CUP performs the best, followed by DNV RP-F101 and PCORRC, with a slight difference in order compared to Table 5. Nevertheless, the ML models outperform the existing empirical models when applied to the PHMSA dataset. While the ML models were trained without utilizing any information from the PHMSA dataset, their generalizability to other datasets may be comparatively weaker. Therefore, the prediction models applied to the PHMSA dataset can be considered generally acceptable, with a recommendation for future data collection to enhance model performance.

6. Conclusion

In this study, a novel methodology for accurately predicting the failure pressure of corroded pipelines using ML algorithms is introduced. This research is distinctive in its incorporation of physically significant features associated with the failure mechanism of corroded pipelines and its careful interpretation of prediction results. The methodology was rigorously developed through an extensive process involving literature review, dataset preparation, and model training, with the resultant ML models being compared to existing empirical models and approaches described in the recent literature. An independent dataset from the PHMSA was utilized to validate the performance of these models.

The ML models developed in this study proved to be exceptionally efficient and accurate in predicting the failure pressures of corroded pipelines. Among these models, the ANN model stood out, exhibiting remarkable metrics, including MAE = 0.842, MAPE = 5.60%, RMSE = 1.188, and R^2 = 0.974. These results clearly demonstrate the superiority of the proposed approach over existing empirical models. The comparison with contemporary literature and the models developed without the proposed features underscores the significance of integrating physical insights into the modeling process to augment the performance of the developed models. To provide further insights into the prediction process, the SHAP method was employed. This method effectively explains the contribution of each parameter to the predicted failure pressure. The analysis revealed that the relative ratio of t/D was the most significant parameter, followed by d/t , defect depth d and pipe thickness t . In contrast, parameters such as width, length, yield strength, and tensile strength had less importance in predicting failure pressure. The ML models outperformed existing empirical models when evaluated using a separate dataset from PHMSA. The study also delved into potential factors contributing to prediction errors, ensuring a comprehensive assessment of model performance.

This research has significant implications for enhancing the design of gas pipelines to prevent corrosion-induced failure and for improving pipeline integrity management practices, offering a powerful and efficient tool for stakeholders in this field. While acknowledging limitations, such as the reliance on a limited dataset and a focus on single corrosion defects, this study provides a foundation for future research.

Future studies are encouraged to employ more comprehensive datasets to enhance model performance and consider scenarios involving multiple corrosion defects, improving the generalizability and applicability of the ML models. Addressing these limitations will contribute to the field and enhance pipeline integrity management practices.

Declaration of Competing Interest

The authors declare that they have no known competing financial interests or personal relationships that could have appeared to influence the work reported in this paper.

Acknowledgment

The first author would like to acknowledge the Joint Postdoc Scheme funded by The Hong Kong Polytechnic University.

References

- Abyani, M., Bahari, M.R., Zarrin, M., Nasseri, M., 2022. Predicting failure pressure of the corroded offshore pipelines using an efficient finite element based algorithm and machine learning techniques. *Ocean Eng.* 254, 111382 <https://doi.org/10.1016/j.oceaneng.2022.111382>.
- Amaya-Gómez, R., Sánchez-Silva, M., Bastidas-Arteaga, E., Schoefs, F., Muñoz, F., 2019a. Reliability assessments of corroded pipelines based on internal pressure – a review. *Eng. Fail. Anal.* 98, 190–214. <https://doi.org/10.1016/j.englfailanal.2019.01.064>.
- Amaya-Gómez, R., Sánchez-Silva, M., Muñoz, F., 2019b. Integrity assessment of corroded pipelines using dynamic segmentation and clustering. *Process Saf. Environ. Prot.* 128, 284–294. <https://doi.org/10.1016/j.psep.2019.05.049>.
- Bea, R.G., 1999. Ram Pipe Requal: A Risk Assessment & Management Based Process For The Requalification Of Marine Pipelines. Presented at the Proceedings Alaskan Arctic Offshore Pipeline Workshop, Anchorage, Alaska.
- Benjamin, A.C., Vieira, R.D., Freire, J.L.F., De Castro, J.T.P., 2000. Burst tests on pipeline with long external corrosion. Volume 2: Integrity and Corrosion; Offshore Issues; Pipeline Automation and Measurement; Rotating Equipment. Presented at the 2000 3rd International Pipeline Conference. American Society of Mechanical Engineers, Calgary, Alberta, Canada. <https://doi.org/10.1115/IPC2000-193>.
- Benjamin, A.C., Andrade, E.Q., 2003. Modified method for the assessment of the remaining strength of corroded pipelines, in: Rio Pipeline 2003 Conference and Exposition, Brazil.
- Benjamin, A.C., Freire, J.L.F., Vieira, R.D., Diniz, J.L.C., De Andrade, E.Q., 2005. Burst Tests on Pipeline Containing Interacting Corrosion Defects, in: 24th International Conference on Offshore Mechanics and Arctic Engineering: Volume 3. Presented at the ASME 2005 24th International Conference on Offshore Mechanics and Arctic Engineering, ASMEDC, Halkidiki, Greece, pp. 403–417. <https://doi.org/10.1115/OMAE2005-67059>.
- Bhardwaj, U., Teixeira, A.P., Guedes Soares, C., 2021. Burst strength assessment of X100 to X120 ultra-high strength corroded pipes. *Ocean Eng.* 241, 110004 <https://doi.org/10.1016/j.oceaneng.2021.110004>.
- Bishop, C.M., 2006. Pattern recognition and machine learning. Information science and statistics. Springer, New York.
- Breiman, L., 2001. Random forests. *Mach. Learn.* 45, 5–32. <https://doi.org/10.1023/A:1010933404324>.
- Chauhan, V., Crossley, J., 2009. Corrosion Assessment Guidance for High Strength Steels (Phase 1).
- Chen, J., Meng, H., Li, Y., 1998. Pipeline prescription analysis after corrosion and explosive test. *Oil Gas Storage Transf.* 28-30+60-5.
- Chen, Y., Zhang, H., Zhang, J., Li, X., Zhou, J., 2015. Failure analysis of high strength pipeline with single and multiple corruptions. *Mater. Des.* 67, 552–557. <https://doi.org/10.1016/j.matdes.2014.10.088>.
- Chen, Z., Li, X., Wang, W., Li, Yan, Shi, L., Li, Yuxing, 2023. Residual strength prediction of corroded pipelines using multilayer perceptron and modified feedforward neural network. *Reliab. Eng. Syst. Saf.* 231, 108980 <https://doi.org/10.1016/j.ress.2022.108980>.
- Choi, J.B., Goo, B.K., Kim, J.C., Kim, Y.J., Kim, W.S., 2003. Development of limit load solutions for corroded gas pipelines. *Int. J. Press. Vessels Pip.* 80, 121–128. [https://doi.org/10.1016/S0308-0161\(03\)00005-X](https://doi.org/10.1016/S0308-0161(03)00005-X).
- Cronin, D.S., Pick, R.J., 2000. Experimental Database for Corroded Pipe: Evaluation of RSTRENG and B31G, in: Volume 2: Integrity and Corrosion; Offshore Issues; Pipeline Automation and Measurement; Rotating Equipment. Presented at the 2000 3rd International Pipeline Conference. American Society of Mechanical Engineers, Calgary, Alberta, Canada, p. V002T06A010. <https://doi.org/10.1115/IPC2000-190>.
- S.Cronin, D., 2000. Assessment of corrosion defects in pipelines. University of Waterloo. CSA Z662:19, Oil and gas pipeline systems, 2019. CSA Group.
- Dawood, T., Elwakil, E., Novoa, H.M., Delgado, J.F.G., 2020. Artificial intelligence for the modeling of water pipes deterioration mechanisms. *Autom. Constr.* 120, 103398 <https://doi.org/10.1016/j.autcon.2020.103398>.
- Diniz, J.L.C., Vieira, R.D., Castro, J.T., Benjamin, A.C., Freire, J.L.F., 2006. Stress and strain analysis of pipelines with localized metal loss. *Exp. Mech.* 46, 765–775. <https://doi.org/10.1007/s11340-006-9826-6>.
- DNV-RP-F101 Corroded pipelines, 2015.
- Fitness-for-Service, FFS-2021, 2022. ASME.
- Fix, E., Hodges, J.L., 1989. Discriminatory analysis. Nonparametric discrimination: consistency properties. *Int. Stat. Rev. Int. Stat.* 57, 238. <https://doi.org/10.2307/1403797>.
- Freire, J.L.F., Vieira, R.D., Castro, J.T.P., Benjamin, A.C., 2006. Part 3: Burst tests of pipeline with extensive longitudinal metal loss. *Exp. Tech.* 30, 60–65. <https://doi.org/10.1111/j.1747-1567.2006.00109.x>.
- Freund, Y., Schapire, R.E., 1995. A desicion-theoretic generalization of on-line learning and an application to boosting. In: Vitányi, P. (Ed.), Computational Learning Theory, Lecture Notes in Computer Science. Springer Berlin Heidelberg, Berlin, Heidelberg, pp. 23–37. https://doi.org/10.1007/s-540-59119-2_166.
- Friedman, J.H., 2001. Greedy function approximation: a gradient boosting machine. *Ann. Stat.* 29 <https://doi.org/10.1214/aos/1013203451>.
- Halim, S.Z., Yu, M., Escobar, H., Quddus, N., 2020. Towards a causal model from pipeline incident data analysis. *Process Saf. Environ. Prot.* 143, 348–360. <https://doi.org/10.1016/j.psep.2020.06.047>.
- Hyndman, R.J., Koehler, A.B., 2006. Another look at measures of forecast accuracy. *Int. J. Forecast.* 22, 679–688. <https://doi.org/10.1016/j.ijforecast.2006.03.001>.
- Kendall, M.G., Stuart, A., Ord, J.K., Arnold, S.F., O'Hagan, A., 1994. Kendall's advanced theory of statistics, 6th ed. ed. Edward Arnold; Halsted Press, London: New York.
- Kere, K.J., Huang, Q., 2022. Development of probabilistic failure pressure models for pipelines with single corrosion defect. *Int. J. Press. Vessels Pip.* 197, 104656 <https://doi.org/10.1016/j.ijpvp.2022.104656>.
- Keshetgar, B., El Amine Ben Seghier, M., 2018. Modified response surface method basis harmony search to predict the burst pressure of corroded pipelines. *Eng. Fail. Anal.* 89, 177–199. <https://doi.org/10.1016/j.englfailanal.2018.02.016>.
- Khan, F., Yarveisy, R., Abbassi, R., 2021. Risk-based pipeline integrity management: a road map for the resilient pipelines. *J. Pipeline Sci. Eng.* 1, 74–87. <https://doi.org/10.1016/j.jpse.2021.02.001>.
- Kiefler, J.F., Maxey, W.A., Eiber, R.J., Duffy, A.R., 1973. Failure Stress Levels of Flaws in Pressurized Cylinders. In: Kaufman, J.G., Swedlow, J.L., Corten, H.T., Srawley, J.E., Heyer, R.H., Wessel, E.T., Irwin, G.R. (Eds.), Progress in Flaw Growth and Fracture Toughness Testing. ASTM International, 100 Barr Harbor Drive, PO Box C700, West Conshohocken, PA 19428-2959, pp. 461–481. <https://doi.org/10.1520/STP49657S>.
- Kim, Yeong-Pyo, Baek, Jong-Hyeon, Kim, U.-Sik, Go, Yeong-Tae, 2002. The evaluation of burst pressure for corroded pipeline by full scale burst test. *Trans. Korean Soc. Mech. Eng. A* 26, 203–210. <https://doi.org/10.3795/KSME-A.2002.26.1.203>.
- Koçak, M., Webster, Janosch, J., Ainsworth, R., Koers, R., 2008. Fitnet Fitness-For-Service (FFs) Procedure. GKSS Research Centre Geesthacht, Germany.
- Li, C., Yang, F., Jia, W., Liu, C., Zeng, J., Song, S., Zhang, Y., 2023. Pipelines reliability assessment considering corrosion-related failure modes and probability distributions characteristic using subset simulation. *Process Saf. Environ. Prot.* 178, 226–239. <https://doi.org/10.1016/j.psep.2023.08.013>.
- Liu, J., Mortimer, L., Wood, A., 2009. Corrosion Assessment Guidance for High Strength Steels (Phase 2).
- Lo, M., Karuppanan, S., Ovinis, M., 2021. Failure pressure prediction of a corroded pipeline with longitudinally interacting corrosion defects subjected to combined loadings using FEM and ANN. *J. Mar. Sci. Eng.* 9, 281. <https://doi.org/10.3390/jmse9030281>.
- Lu, H., Iseley, T., Matthews, J., Liao, W., Azimi, M., 2021a. An ensemble model based on relevance vector machine and multi-objective salp swarm algorithm for predicting burst pressure of corroded pipelines. *J. Pet. Sci. Eng.* 203, 108585 <https://doi.org/10.1016/j.petrol.2021.108585>.
- Lu, H., Xu, Z.-D., Iseley, T., Matthews, J.C., 2021b. Novel data-driven framework for predicting residual strength of corroded pipelines. *J. Pipeline Syst. Eng. Pract.* 12, 04021045 [https://doi.org/10.1061/\(ASCE\)PS.1949-1204.0000587](https://doi.org/10.1061/(ASCE)PS.1949-1204.0000587).
- Lundberg, S.M., Lee, S.-I., 2017. A Unified Approach to Interpreting Model Predictions. Presented at the 31st Conference on Neural Information Processing Systems, Long Beach, CA, USA, p. 10.
- Lundberg, S.M., Erion, G., Chen, H., DeGrave, A., Prutkin, J.M., Nair, B., Katz, R., Himmelfarb, J., Bansal, N., Lee, S.-I., 2020. From local explanations to global understanding with explainable AI for trees. *Nat. Mach. Intell.* 2, 56–67. <https://doi.org/10.1038/s42256-019-0138-9>.
- Ma, B., Shuai, J., Liu, D., Xu, K., 2013. Assessment on failure pressure of high strength pipeline with corrosion defects. *Eng. Fail. Anal.* 32, 209–219. <https://doi.org/10.1016/j.englfailanal.2013.03.015>.
- Ma, H., Zhang, W., Wang, Y., Ai, Y., Zheng, W., 2023b. Advances in corrosion growth modeling for oil and gas pipelines: a review. *Process Saf. Environ. Prot.* 171, 71–86. <https://doi.org/10.1016/j.psep.2022.12.054>.
- Ma, H., Wang, H., Geng, M., Ai, Y., Zhang, W., Zheng, W., 2023a. A new hybrid approach model for predicting burst pressure of corroded pipelines of gas and oil. *Eng. Fail. Anal.* 149, 107248 <https://doi.org/10.1016/j.englfailanal.2023.107248>.
- Ma, Y., Zheng, J., Liang, Y., Klemeš, J.J., Du, J., Liao, Q., Lu, H., Wang, B., 2022. Deeppipe: theory-guided neural network method for predicting burst pressure of corroded pipelines. *Process Saf. Environ. Prot.* 162, 595–609. <https://doi.org/10.1016/j.psep.2022.04.036>.
- Mannucci, G., Demofonti, G., Barsanti, L., Harris, D., Hillenbrand, H.G., 2002. Fracture properties of API X 100 gas pipeline steels: final report. *Dir.-Gen. Res. Innov.*
- Manservigi, L., Bahlawan, H., Losi, E., Morini, M., Spina, P.R., Venturini, M., 2022. A diagnostic approach for fault detection and identification in district heating networks. *Energy* 251, 123988. <https://doi.org/10.1016/j.energy.2022.123988>.
- Manual for determining the remaining strength of corroded pipelines: a supplement to ASME B31 code for pressure piping: an American National Standard, Revision of ASME B31G-2009, ed. 2012. American Society of Mechanical Engineers, New York, N.Y.

- Mok, D.H.B., Pick, R.J., Glover, A.G., Hoff, R., 1991. Bursting of line pipe with long external corrosion. *Int. J. Press. Vessels Pip.* 46, 195–216. [https://doi.org/10.1016/0308-0161\(91\)90015-T](https://doi.org/10.1016/0308-0161(91)90015-T).
- Muhlbauer, W.K., 2006. Pipeline risk management manual: ideas, techniques, and resources, 3. ed. ed. Elsevier, Amsterdam.
- Netto, T.A., Ferraz, U.S., Estefen, S.F., 2005. The effect of corrosion defects on the burst pressure of pipelines. *J. Constr. Steel Res.* 61, 1185–1204. <https://doi.org/10.1016/j.jcsr.2005.02.010>.
- Oh, C.-K., Kim, Y.-J., Baek, J.-H., Kim, Y.-P., Kim, W.-S., 2007. Ductile failure analysis of API X65 pipes with notch-type defects using a local fracture criterion. *Int. J. Press. Vessels Pip.* 84, 512–525. <https://doi.org/10.1016/j.ijpvp.2007.03.002>.
- Oh, D., Race, J., Oterkus, S., Koo, B., 2020. Burst pressure prediction of API 5L X-grade dented pipelines using deep neural network. *J. Mar. Sci. Eng.* 8, 766. <https://doi.org/10.3390/jmse8100766>.
- Phan, H.C., Dhar, A.S., 2021. Predicting pipeline burst pressures with machine learning models. *Int. J. Press. Vessels Pip.* 191, 104384 <https://doi.org/10.1016/j.ijpvp.2021.104384>.
- Phan, H.C., Duong, H.T., 2021. Predicting burst pressure of defected pipeline with principal component analysis and adaptive neuro fuzzy inference system. *Int. J. Press. Vessels Pip.* 189, 104274 <https://doi.org/10.1016/j.ijpvp.2020.104274>.
- PHMSA, 2023. Pipeline Incident Flagged Files [WWW Document]. URL <https://www.phmsa.dot.gov/data-and-statistics/pipeline/data-and-statistics-overview>.
- Quinlan, J.R., 1986. Induction of decision trees. *Mach. Learn.* 1, 81–106. <https://doi.org/10.1007/BF00116251>.
- Ritchie, D., Last, S., 1995. Burst criteria of corroded pipelines-defect acceptance criteria. Presented at the Proceedings of the EPRG/PRC 10th biennial joint technical meeting on line pipe research, pp. 1–11.
- Shuai, Y., Shuai, J., Xu, K., 2017. Probabilistic analysis of corroded pipelines based on a new failure pressure model. *Eng. Fail. Anal.* 81, 216–233. <https://doi.org/10.1016/j.engfailanal.2017.06.050>.
- Silva, R.C.C., Guerreiro, J.N.C., Loula, A.F.D., 2007. A study of pipe interacting corrosion defects using the FEM and neural networks. *Adv. Eng. Softw.* 38, 868–875. <https://doi.org/10.1016/j.advengsoft.2006.08.047>.
- Souza, R.D., Benjamin, A.C., Vieira, R.D., Freire, J.L.F., Castro, J.T.P., 2007. Part 4: Rupture tests of pipeline segments containing long real corrosion defects. *Exp. Tech.* 31, 46–51. <https://doi.org/10.1111/j.1747-1567.2006.00134.x>.
- Stephens, D.R., Leis, B.N., 2000. Development of an alternative criterion for residual strength of corrosion defects in moderate- to high-toughness pipe. Volume 2: Integrity and Corrosion; Offshore Issues; Pipeline Automation and Measurement; Rotating Equipment. Presented at the 2000 3rd International Pipeline Conference. American Society of Mechanical Engineers, Calgary, Alberta, Canada. <https://doi.org/10.1115/IPC2000-192>.
- Su, Y., Li, J., Yu, B., Zhao, Y., Yao, J., 2021. Fast and accurate prediction of failure pressure of oil and gas defective pipelines using the deep learning model. *Reliab. Eng. Syst. Saf.* 216, 108016 <https://doi.org/10.1016/j.ress.2021.108016>.
- Vapnik, V.N., 1995. *The nature of statistical learning theory*. Springer, New York.
- Wang, H., Yajima, A., Castaneda, H., 2019. A stochastic defect growth model for reliability assessment of corroded underground pipelines. *Process Saf. Environ. Prot.* 123, 179–189. <https://doi.org/10.1016/j.psep.2019.01.005>.
- Wang, X., Mazumder, R.K., Salarieh, B., Salman, A.M., Shafeezadeh, A., Li, Y., 2022. Machine learning for risk and resilience assessment in structural engineering: progress and future trends. *J. Struct. Eng.* 148, 03122003 [https://doi.org/10.1061/\(ASCE\)ST.1943-541X.0003392](https://doi.org/10.1061/(ASCE)ST.1943-541X.0003392).
- Wang, Y., Zhang, Z., Liu, S., Xia, A., Li, R., Qin, G., 2023. Importance sampling-based probabilistic performance modeling of low-, mid- and high-strength pipelines under coupling effect of hydrogen-induced damage and corrosion. *Process Saf. Environ. Prot.* 180, 428–442. <https://doi.org/10.1016/j.psep.2023.10.021>.
- Xie, M., Zhao, J., Pei, X., 2023. Maintenance strategy optimization of pipeline system with multi-stage corrosion defects based on heuristically genetic algorithm. *Process Saf. Environ. Prot.* 170, 553–572. <https://doi.org/10.1016/j.psep.2022.12.041>.
- Yeom, K.J., Lee, Y.-K., Oh, K.H., Kim, W.S., 2015a. Integrity assessment of a corroded API X70 pipe with a single defect by burst pressure analysis. *Eng. Fail. Anal.* 57, 553–561. <https://doi.org/10.1016/j.engfailanal.2015.07.024>.
- Yeom, K.J., Lee, Y.-K., Oh, K.H., Kim, W.S., 2015b. Integrity assessment of a corroded API X70 pipe with a single defect by burst pressure analysis. *Eng. Fail. Anal.* 57, 553–561. <https://doi.org/10.1016/j.engfailanal.2015.07.024>.
- Yeom, K.J., Lee, Y.-K., Oh, K.H., Kim, W.S., 2015c. Integrity assessment of a corroded API X70 pipe with a single defect by burst pressure analysis. *Eng. Fail. Anal.* 57, 553–561. <https://doi.org/10.1016/j.engfailanal.2015.07.024>.
- Zhang, T., Shuai, J., Shuai, Y., Hua, L., Xu, K., Xie, D., Mei, Y., 2023. Efficient prediction method of triple failure pressure for corroded pipelines under complex loads based on a backpropagation neural network. *Reliab. Eng. Syst. Saf.* 231, 108990 <https://doi.org/10.1016/j.ress.2022.108990>.
- Zhu, X.-K., 2021. A comparative study of burst failure models for assessing remaining strength of corroded pipelines. *J. Pipeline Sci. Eng.* 1, 36–50. <https://doi.org/10.1016/j.jpse.2021.01.008>.
- Zhu, X.-K., 2023. Exact solution of burst pressure for thick-walled pipes using the flow theory of plasticity. *Int. J. Mech. Sci.* 259, 108582 <https://doi.org/10.1016/j.ijmecsci.2023.108582>.
- Zio, E., 2022. Prognostics and Health Management (PHM): where are we and where do we (need to) go in theory and practice. *Reliab. Eng. Syst. Saf.* 218, 108119 <https://doi.org/10.1016/j.ress.2021.108119>.